Journal of the Korean Physical Society
https://doi.org/10.1007/s40042-025-01503-6

Online ISSN 1976-8524
Print ISSN 0374-4884

RESEARCH - STATISTICAL PHYSICS

Exploring optical soliton solution for (2+ 1)-dimensional Kundu–Mukherjee–Naskar equation using two analytical methods with sensitivity analysis

Muhammad Imran Asjad[1,2,3] · Azad Ali Sagher[1] · Muhammad Bilal Riaz[4,5] · Suhad Ali Osman Abdallah[6]

Received: 17 May 2025 / Revised: 1 September 2025 / Accepted: 29 September 2025

Abstract

This study develops exact soliton solutions for the (2+1)-dimensional Kundu–Mukherjee– Naskar equation, a versatile model describing signal transmission in telecommunications and long-distance optical fiber pulse propagation. The equation is reduced to a nonlinear ordinary differential form using a traveling wave transformation derived from Lie symmetry infinitesimals. Two analytical approaches, the modified Sardar sub-equation method and the modified auxiliary equation method, are applied to obtain diverse classes of solutions, including hyperbolic, Jacobi, trigonometric, and rational forms. Numerical simulations, performed in MATLAB, visualize bright, dark, singular, kink, periodic, and anti-kink soliton structures through 3D, 2D, and density plots. The sensitivity of the dynamical system to changes in initial conditions is analyzed, with Lyapunov exponents computed to quantify its stability and dynamic complexity. Both qualitative and quantitative perspectives are considered. The results are significant for optical fiber communications, where such stable soliton solutions can minimize signal distortion, enhance transmission quality, and support high-capacity, long-distance data transfer.

Keywords Modified auxiliary equation method · Modified Sardar sub equation method · Soliton · Sensitivity analysis

1 Introduction

Nonlinear partial differential equations (NLPDE) are also known as nonlinear mathematical physics equations or nonlinear evolution. Nonlinear phenomena occur in a wide range of significant scientific and mathematical fields, including physical chemistry, biology, and atmospheric and space sciences. [1–8]. In recent years, partial differential equations (PDEs) have found numerous applications in physics, applied mathematics, astronomy, and a variety of other sciences. PDEs are useful modeling tools in a variety of natural science and engineering disciplines. They hold enormous potential for boosting scientific studies. PDEs have gained importance in applied mathematics in recent years. PDEs are constructed by mathematical modeling of natural phenomena that describe the dynamics of this scientific event that appears in nature.

Soliton theory is a key topic in mathematical physics and applied mathematics, fields that have advanced quickly since the 1960s. Solitons, sometimes referred to as solitary waves, are found in the solutions of a number of partial differential equations that are nonlinear. They can be used to explain a number of significant physical events and have a number of exceptional qualities. Nowadays, the idea of soliton has also

✉ Azad Ali Sagher
azadali8282@gmail.com

[1] Department of Mathematics, University of Management and Technology, 54770 Lahore, Pakistan

[2] Center for Theoretical Physics, Khazar University, 41 Mehseti str., Baku, AZ 1096, Azerbaijan

[3] Jadara University Research Center, Jadara University, Irbid, Jordan

[4] IT4 Innovations, VSB Technical University of Ostrava, Ostrava, Czech Republic

[5] Applied Science Research Center, Applied Science Private University, Amman, Jordan

[6] Applied College, Khamis Mushait, King Khalid University, Abha 62529, Saudi Arabia

Published online: 14 October 2025

come to be examined in a wider context. Several NLPDE researchers have employed a range of techniques to produce solitary traveling wave solutions in previous studies. In [9], Feng et al. constructed wave solutions, such as bright, dark, and kink solitons, using the Hirota bilinear technique. Better findings came from later studies conducted by researchers such as [10] and [11]. To find the soliton solution, [12] examines the sine-cosine and sinh-cosh methods. Atas et al. [13] explored some novel wave solutions using the modified generalized exp rational approach. The representation of the generalized Riccati equation for the Fokas system was examined by Kumar and Kumar in [14]. There are many methods to study the partial differential equations (PDEs) in the sense of soliton wave theory. Using the Khater II method, Khater obtained exact wave soliton solutions in [16]. In [17], Zayed et al. explored a nonlinear model to get dark, singular, bright, and dark-singular solitons. In [18], the new extended technique was utilized to construct the novel wave solution. In [19], unique solitary wave solutions were discovered via the Sardar Sub-equation methodology, the Khater II strategy, and the new extended Kudryashov method. Majid et al. [20] developed bright, periodic, multiple bright-periodic, mixed, and multiple bright-dark. Majid et al. analyzed a variety of solitary wave solutions via generalized projective Riccati equations, such as U-shaped, bright, bell-shaped, dark, and flat kink-type peaks, using in [26]. The Kolmogorov–Petrovsky–Piskunov (KPP) model's soliton solutions with a time-dependent variable coefficient were investigated in [27]. Several new optical soliton solutions, such as periodic waves, kink-type waves, rogue-type waves, and unique periodic waves, were created in [28] by providing suitable fractional parametric values.

In 2013, Kundu and Mukherjee [29] explored the higher-order nonlinear Schrödinger equation along with its characteristics and applications in various fields of science and engineering. The following year, Kundu et al. [30] introduced the (2+1)-dimensional Kundu–Mukherjee–Naskar (KMN) equation and its soliton wave solutions, which have since been extensively studied by many researchers. In ocean engineering, wave phenomena are crucial for understanding marine dynamics, while in optics and fiber technology, such equations describe nonlinear wave propagation [31–34]. In fiber-optic communications, optical solitons predicted by these models enable high-speed, long-distance data transmission with minimal distortion, outperforming conventional electrical systems. Considering these applications, we now focus on the KMN equation [36], which is described by the following form:

$$i\mathcal{L}_t + \lambda_1 \mathcal{L}_{xy} + i\lambda_2\left(\mathcal{L}\mathcal{L}_x^* - \mathcal{L}^*\mathcal{L}_x\right) = 0, \quad i = \sqrt{-1}, \tag{1}$$

which models the evolution of a complex wave envelope $\mathcal{L}(x, y, t)$ propagating in a two-dimensional spatial domain, where x and y are spatial coordinates and t denotes time. The imaginary unit $i = \sqrt{-1}$ reflects the inherently oscillatory and wave-like nature of the system.

- The term $i\mathcal{L}_t$ describes the time evolution of the wave envelope with a complex phase factor, typical in Schrödinger-type wave equations.
- The dispersive effects are represented by $\lambda_1 \mathcal{L}_{xy}$, a mixed second-order spatial derivative. This term models the spreading and shape change of the wave packet due to dispersion, involving coupling between the spatial variables x and y.
- The nonlinear term $i\lambda_2\left(\mathcal{L}\mathcal{L}_x^* - \mathcal{L}^*\mathcal{L}_x\right)$ accounts for nonlinear self-interaction effects, such as self-steepening or nonlinear phase modulation. It involves the wave envelope $\mathcal{L}$ and its spatial derivative, as well as their complex conjugates, reflecting the nonlinear influence on wave amplitude and phase.
- $\mathcal{L}\mathcal{L}_x^*$ represents how the wave amplitude couples to the spatial derivative of the conjugate, capturing phase-gradient effects and $\mathcal{L}^*\mathcal{L}_x$ is the reverse coupling.

Physically, this can describe self-induced drift or self-steepening effects, where the phase gradients alter wave motion. This equation resembles nonlinear dispersive wave models found in nonlinear optics, plasma physics, and shallow water waves, with a key difference: instead of the usual Kerr nonlinearity $|\mathcal{L}|^2\mathcal{L}$, the nonlinear term depends on spatial phase gradients. This allows the model to capture effects such as refractive index changes driven by intensity gradients in non-Kerr media, nonreciprocal coupling in anisotropic materials, and two-dimensional modulational instabilities with phase-sensitive interactions.

In fresh work [31–34], different solutions for optical pulses have been proposed for the Eq. (1). Kumar et al. [35] discussed this problem by oblique wave propagation. Jhangeer et al. [36] have derived the complex wave solution with the aid of a new extended algebraic method approach. In [37], the periodic property and its stability analysis were studied in the sense of fractional. With the aid of the Laplace Adomian decomposition method, the Eq. (1) was investigated [38]. The optical solitons are reported for the Eq. (1) model in [39–43].

From the above information, we find the research gap: the modified Sardar sub-equation (MSSE) method [44] and the modified auxiliary equation (MAE) method [45, 47] have not been studied previously. Murad et al. [48] used the MSSE method to solve the Fokas–Lenells equation, and Kamel et al. [49] also applied this method to the nonlinear Schrödinger equation. Akram et al.[50] explored the Lakshmanan–Porsezian–Daniel (LPD) model with the MAE method. These methods are effective for deriving exact solutions in lower-dimensional nonlinear models. However, they

encounter limitations when applied to higher-dimensional systems, where the mathematical structure becomes more intricate due to multi-directional wave interactions and strong nonlinear couplings. In such cases, the solvability of these methods is restricted, and the resulting solutions may not fully capture the complex dynamical behavior of the model. Therefore, while they remain useful for certain classes of equations, their applicability to higher-dimensional frameworks is limited, necessitating the development or adoption of more generalized analytical techniques and advanced computational approaches. Additionally, none of the researchers discussed the sensitivity visualizations for this model to check the parametric impact and Lyapunov exponents in the past. This demonstrates a significant gap in earlier research. The work we do closes this gap by incorporating various advanced methodologies and doing an in-depth review of the model. These methods are employed for the first time to provide an exact solution to the KMN model. There are various optical soliton patterns obtained, including bright shapes, dark shapes, and singular solitons in the shape of hyperbolic, exponential, trigonometric, and rational forms when we visualized some wave solutions obtained by (MSSE) method. While the visualization of the MAE method describes the wave solution in the form of a kink shaped, periodic, and anti kink pattern [51]. The interesting and useful aspects of acquired optical solitons in the evolutionary dynamics help us understand complex physical phenomena. After careful analysis, we use the Galilean transformation to create a dynamical system, a first-order ODE. Using this dynamic system, we analyze the model's sensitivity analysis and Lyapunov exponents under various initial conditions.

The setup of the current article is as follows: Sect. 2 describes the algorithm of both the MSSE method and the MAE method. In Sect. 3, it explores the implementation of both these techniques to consider models and their visual presentations. In Sect. 4, it discusses the explanation of visualization. In Sect. 5, we discuss the dynamical study in the aspect of sensitivity analysis, Lyapunov exponents and comparison of wave solutions of both these methods and with previous studies. Finally, Sect. 6 gives the concluding remarks.

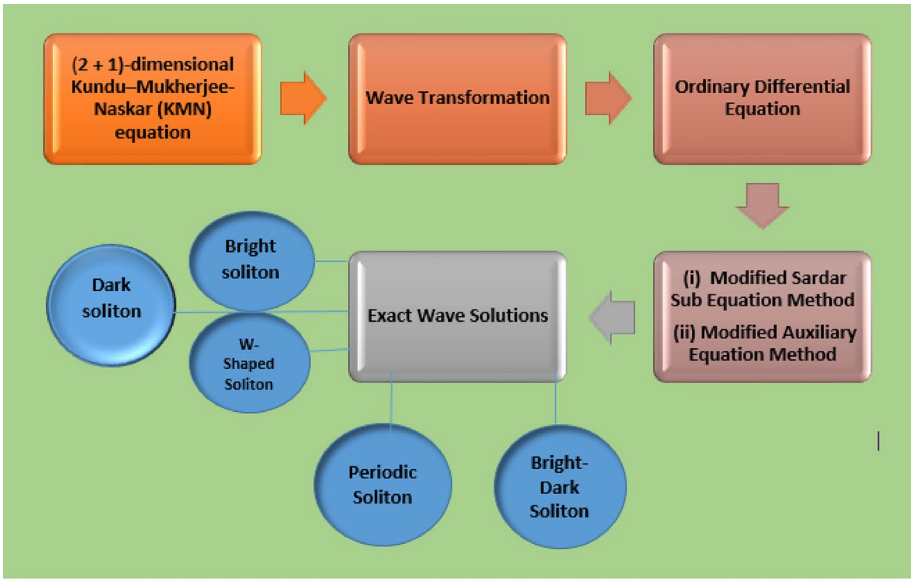

(a) Flow chart of our novel work

2 Algorithm of techniques

In this section of the current study, we develop the algorithm of both methods. Considered the nonlinear partial differential equation (NPDE) of the form:

$$S\left(z, z_x, z_t, z_{xx}, z_{xt}, \dots\right) = 0, \tag{2}$$

where $z = z(x,t)$ is an unknown function. Applying the following transformation the Eq. (1) change into ODE

$$z(x,t) = W(cx + \mathrm{d}y + \omega t), \quad \tau = x - \nu t, \tag{3}$$

$$T\left(z, z', z'', z''', ..., \dots\right) = 0, \tag{4}$$

2.1 The modified Sardar sub-equation technique

As per technique [44], the general solution of Eq. (4) in the form of

$$W(\tau) = R_0 + \sum_{i=1}^{N} R_i P^i(\tau), \quad R_i \neq 0, \tag{5}$$

where $W = W(\tau)$, The solutions of Eq. (5) are satisfied by the following equation in the form of:

$$P'(\tau)^2 = \epsilon_2 P(\tau)^4 + \epsilon_1 P(\tau)^2 + \epsilon_0, \tag{6}$$

where $\epsilon_0 \neq 1$ and ϵ_1 and $\epsilon_2 \neq 0$ are considered to be integers. To set the R_i to be zero we find out the values of the constants R_0, R_1, and R_2. Find out the value of N using the homogeneous balance principle. Following are the solutions to Equation (6).

Case 1:

- If $\epsilon_0 = 0, \epsilon_1 > 0$, and $\epsilon_2 \neq 0$, then

$$P_1(\tau) = \sqrt{-\frac{\epsilon_1}{\epsilon_2}}\,\mathrm{sech}\left(\sqrt{\epsilon_1}(\eta + \tau)\right), \tag{7}$$

- If $\epsilon_0 = 0, \epsilon_1 > 0$, and $\epsilon_2 \neq 0$, then

$$P_2(\tau) = \sqrt{-\frac{\epsilon_1}{\epsilon_2}}\,\mathrm{csch}\left(\sqrt{\epsilon_1}(\eta + \tau)\right). \tag{8}$$

Case 2:

- For constants f_1 and f_2, let $\epsilon_0 = 0$, $\epsilon_1 > 0$, and $\epsilon_2 = +4f_1f_2$; then,

$$P_3(\tau) = \frac{4f_1\sqrt{\epsilon_1}}{\left(4f_1^2 - \epsilon_2\right)\sinh\left(\sqrt{\epsilon_1}(\eta + \tau)\right) + \left(4f_1^2 - \epsilon_2\right)\cosh\left(\sqrt{\epsilon_1}(\eta + \tau)\right)}. \tag{9}$$

Case 3:

- For constants R_1 and R_2, let $\epsilon_0 = \frac{\epsilon_1^2}{4\epsilon_2}$, $\epsilon_1 < 0$, and $\epsilon_2 > 0$;

- If $\epsilon_0 = 0, \epsilon_1 > 0$, and $\epsilon_2 \neq 0$, then

$$P_4(\tau) = \sqrt{-\frac{\epsilon_1}{2\epsilon_2}}\tanh\left(\sqrt{-\frac{\epsilon_1}{2}}(\eta + \tau)\right). \tag{10}$$

- For constants R_1 and R_2, let $\epsilon_0 = \frac{\epsilon_1^2}{4\epsilon_2}$, $\epsilon_1 < 0$, and $\epsilon_2 > 0$; then

$$P_5(\tau) = \sqrt{-\frac{\epsilon_1}{2\epsilon_2}}\coth\left(\sqrt{-\frac{\epsilon_1}{2}}(\eta + \tau)\right). \tag{11}$$

- For constants R_1 and R_2, let $\epsilon_0 = \frac{\epsilon_1^2}{4\epsilon_2}$, $\epsilon_1 < 0$, and $\epsilon_2 > 0$; then

$$P_6(\tau) = \sqrt{-\frac{\epsilon_1}{2\epsilon_2}}\left(\tanh\left(\sqrt{-\frac{\epsilon_1}{2}}(\eta + \tau)\right) + \mathrm{sech}\left(\sqrt{-2\epsilon_1}(\eta + \tau)\right)\right). \tag{12}$$

- For constants R_1 and R_2, let $\epsilon_0 = \frac{\epsilon_1^2}{4\epsilon_2}$, $\epsilon_1 < 0$, and $\epsilon_2 > 0$; then

$$P_7(\tau) = \sqrt{-\frac{\epsilon_1}{8\epsilon_2}}\left(\tanh\left(\sqrt{-\frac{\epsilon_1}{8}}(\eta + \tau)\right) + \coth\left(\sqrt{-\frac{\epsilon_1}{8}}(\eta + \tau)\right)\right). \tag{13}$$

- For constants R_1 and R_2, let $\epsilon_0 = \frac{\epsilon_1^2}{4\epsilon_2}$, $\epsilon_1 < 0$, and $\epsilon_2 > 0$; then

$$P_8(\tau) = \sqrt{-\frac{\epsilon_1}{2\epsilon_2}}\cosh\left(\sqrt{-2\epsilon_1}(\eta + \tau)\right) \sinh\left(\sqrt{-2\epsilon_1}(\eta + \tau)\right) + i. \tag{14}$$

Case 4:

- Let $\epsilon_0 = 0, \epsilon_1 < 0$, and $\epsilon_2 \neq 0$; then

$$P_9(\tau) = \sqrt{-\frac{\epsilon_1}{\epsilon_2}}\sec\left(\sqrt{-\epsilon_1}(\eta + \tau)\right). \tag{15}$$

- Let $\epsilon_0 = 0, \epsilon_1 < 0$, and $\epsilon_2 \neq 0$; then

$$P_{10}(\tau) = \sqrt{-\frac{\epsilon_1}{\epsilon_2}}\ \csc\left(\sqrt{-\epsilon_1}(\eta+\tau)\right). \tag{16}$$

Case 5:

- Let $\epsilon_0 = \frac{\epsilon_1^2}{4\epsilon_2}$, $\epsilon_1 > 0$, $\epsilon_2 > 0$, and $R_1^2 - R_2^2 > 0$; then

$$P_{11}(\tau) = \sqrt{-\frac{\epsilon_1}{2\epsilon_2}}\ \tan\left(\sqrt{\frac{\epsilon_1}{2}}(\eta+\tau)\right). \tag{17}$$

- Let $\epsilon_0 = \frac{\epsilon_1^2}{4\epsilon_2}$, $\epsilon_1 > 0$, $\epsilon_2 > 0$, and $R_1^2 - R_2^2 > 0$; then

$$P_{12}(\tau) = -\sqrt{-\frac{\epsilon_1}{2\epsilon_2}}\ \cot\left(\sqrt{\frac{\epsilon_1}{2}}(\eta+\tau)\right). \tag{18}$$

- Let $\epsilon_0 = \frac{\epsilon_1^2}{4\epsilon_2}$, $\epsilon_1 > 0$, $\epsilon_2 > 0$, and $R_1^2 - R_2^2 > 0$; then

$$\begin{aligned} P_{13}(\tau) = &-\sqrt{-\frac{\epsilon_1}{2\epsilon_2}}\Big(\tan\left(\sqrt{2\epsilon_1}(\eta+\tau)\right) \\ &-\sec\left(\sqrt{2\epsilon_1}(\eta+\tau)\right)\Big). \end{aligned} \tag{19}$$

- Let $\epsilon_0 = \frac{\epsilon_1^2}{4\epsilon_2}$, $\epsilon_1 > 0$, $\epsilon_2 > 0$, and $R_1^2 - R_2^2 > 0$; then

$$\begin{aligned} P_{14}(\tau) = &\sqrt{-\frac{\epsilon_1}{8\epsilon_2}}\Bigg(\tan\left(\sqrt{\frac{\epsilon_1}{8}}(\eta+\tau)\right) \\ &-\cot\left(\sqrt{\frac{\epsilon_1}{8}}(\eta+\tau)\right)\Bigg). \end{aligned} \tag{20}$$

- Let $\epsilon_0 = \frac{\epsilon_1^2}{4\epsilon_2}$, $\epsilon_1 > 0$, $\epsilon_2 > 0$, and $R_1^2 - R_2^2 > 0$; then

$$P_{15}(\tau) = \frac{\sqrt{-\frac{\epsilon_1}{2\epsilon_2}}\left(\sqrt{R_1^2 - R_2^2 - W_1\cos\left(\sqrt{2\epsilon_1}(\eta+\tau)\right)}\right)}{\left(R_2 + W_1\sin\left(\sqrt{2\epsilon_1}(\eta+\tau)\right)\right)}, \tag{21}$$

$$\begin{aligned} P_{16}(\tau) = &\sqrt{-\frac{\epsilon_1}{2\epsilon_2}}\ \cos\left(\sqrt{2\epsilon_1}(\eta+\tau)\right) \\ &\sin\left(\sqrt{2\epsilon_1}(\eta+\tau)\right) - 1. \end{aligned} \tag{22}$$

Case 6:

- Let $\epsilon_0 = 0$ and $\epsilon_1 > 0$; then

$$P_{17}(\tau) = \frac{4\epsilon_1 e^{\sqrt{\epsilon_1}(\eta+\tau)}}{e^{2\sqrt{\epsilon_1}(\eta+\tau)} - 4\epsilon_1\epsilon_2}. \tag{23}$$

- Let $\epsilon_0 = 0$ and $\epsilon_1 > 0$; then

$$P_{18}(\tau) = \frac{4\epsilon_1 e^{\sqrt{\epsilon_1}(\eta+\tau)}}{1 - 4\epsilon_1\epsilon_2 e^{2\sqrt{\epsilon_1}(\eta+\tau)}}. \tag{24}$$

Case 7:

- Let $\epsilon_0 = 0$, $\epsilon_1 = 0$, and $\epsilon_2 > 0$; then

$$H_{19}(\tau) = \frac{1}{\sqrt{\epsilon_2(\eta+\tau)}}. \tag{25}$$

- Let $\epsilon_0 = 0$, $\epsilon_1 = 0$, and $\epsilon_2 > 0$; then

$$P_{20}(\tau) = i\sqrt{\epsilon_2(\eta+\tau)}. \tag{26}$$

2.2 Modified auxiliary equation method

The homogeneous balance algorithm is utilized to determine the balance number $n = 1$ in Eq. (35). According to the modified auxiliary equation method [45], we can suppose the following solution:

$$\begin{aligned} U(\tau) =& m_0 + \sum_{i=1}^{n}\left(m_i(Q^f)^i + n_i(Q^f)^{-i}\right) \\ =& m_0 + m_1 Q^f + n_1 Q^{-f}, \end{aligned} \tag{27}$$

where $f(\tau)$ satisfies the following auxiliary equation and constants m_0, m_i and n_i need to be calculated.

$$f'(\tau) = \frac{\beta_1 + \alpha_1 Q^{-f} + \sigma_1 Q^f}{ln(g)}. \tag{28}$$

where σ_1, β_1, α_1, and g are unspecified constants with $g > 0$ and $g \neq 1$. The results of Eq. (28) are as follows:

- If $\beta_1^2 - 4\sigma_1\alpha_1 < 0$ and $\sigma_1 \neq 0$,

$$Q^{f(\tau)} = \frac{-\beta_1 + \sqrt{4\sigma_1\alpha_1 - \beta_1^2}\ \tan\left(\frac{\sqrt{4\sigma_1\alpha_1 - \beta_1^2}\,\tau}{2}\right)}{2\sigma_1} \tag{29}$$

or

$$Q^{f(\tau)} = \frac{-\beta_1 + \sqrt{4\sigma_1\alpha_1 - \beta_1^2}\ \cot\left(\frac{\sqrt{4\sigma_1\alpha_1 - \beta_1^2}\,\tau}{2}\right)}{2\sigma_1}. \tag{30}$$

- If $\beta_1^2 - 4\sigma_1\alpha_1 > 0$ and $\sigma_1 \neq 0$,

$$Q^{f(\tau)} = \frac{-\beta_1 + \sqrt{\beta_1^2 - 4\sigma_1\alpha_1}\ \tanh\left(\frac{\sqrt{\beta_1^2 - 4\sigma_1\alpha_1}\,\tau}{2}\right)}{2\sigma_1} \tag{31}$$

or

$$Q^{f(\tau)} = \frac{-\beta_1 + \sqrt{\beta_1^2 - 4\sigma_1\alpha_1}\coth\left(\frac{\sqrt{\beta_1^2-4\sigma_1\alpha_1}\,\tau}{2}\right)}{2\sigma_1}. \tag{32}$$

- If $\beta_1^2 - 4\sigma_1\alpha_1 = 0$,

$$Q^{f(\tau)} = \frac{-2 + \beta_1\tau}{2\sigma_1\tau}. \tag{33}$$

3 Execution of the proposed methods

We adopted the MSSE method and MAE method in this part of the current article for the MKN model to construct the soliton wave solution.

3.1 The modified Sardar sub-equation technique

The modified Sardar sub-equation Technique is applied to solve the Eq. (1), beginning with the following assumptions. The first step in employing this strategy is to minimize the equation's complexity through smart substitution of wave variables. These variables are carefully chosen to convert the equation into a more tractable form that can be solved exactly. Simplification using appropriate wave variables is critical for enabling the method's use. Under the stated assumptions, we proceed to derive wave solutions to Eq. (1) by the following analysis.

$$\begin{aligned}\mathcal{Y}(x,y,t) =& \mathcal{Y}(\vartheta)\times\exp(i\tau),\\ \vartheta =& ax + by - t, \quad \tau = cx + \mathrm{d}y + \omega t.\end{aligned} \tag{34}$$

where τ and ℓ are undetermined values.

Substituting Eq. (34) into Eq. (1) and separating it into real and imaginary parts yields

$$\lambda_1 ab\frac{d^2\mathcal{Y}(\vartheta)}{d\vartheta^2} - \left(\omega + \lambda_1 cd\right)\mathcal{Y}(\vartheta) + 2c\lambda_2\mathcal{Y}^3(\vartheta) = 0. \tag{35}$$

and

$$\theta = \lambda_1(ad + bc). \tag{36}$$

Using the homogeneous balancing algorithm [46] gives the simple equation $M + 2 = 3M$. We find M = 1. Thus, the solutions of the KMN model in (5) can be written in the form with this balance value $M = 1$.

$$W(\tau) = R_0 + R_1 P(\tau), \tag{37}$$

The constants R_0 and R_1 will be established later. Substituting Eqs. (37) and (6) into Eq. (35) and equating the coefficients of different powers of P to zero results in a system of nonlinear algebraic equations. Solving this algebraic equation yields the following set of solutions.

$$\begin{aligned}R_1 =& \pm\sqrt{-\frac{ab\epsilon_2\omega}{abc\epsilon_1\lambda_2 - c^2d\lambda_2}}, R_0 = 0,\\ \lambda_1 =& \frac{\omega}{ab\epsilon_1 - cd}.\end{aligned} \tag{38}$$

Family 1: If $\epsilon_0 = 0$, $\epsilon_1 > 0$, and $\epsilon_2 \neq 0$;

$$\begin{aligned}W_1(x,y,t) =& \left(\pm\sqrt{-\frac{ab\epsilon_2\omega}{abc\epsilon_1\lambda_2 - c^2d\lambda_2}}\right)\sqrt{-\frac{\epsilon_1}{\epsilon_2}}\\ & \operatorname{sech}\left(\sqrt{\epsilon_1}(\eta + cx + \mathrm{d}y + \omega t)\right).e^{i(cx+\mathrm{d}y+\omega t)},\end{aligned} \tag{39}$$

$$\begin{aligned}W_2(x,y,t) =& \left(\pm\sqrt{-\frac{ab\epsilon_2\omega}{abc\epsilon_1\lambda_2 - c^2d\lambda_2}}\right)\sqrt{-\frac{\epsilon_1}{\epsilon_2}}\\ & \operatorname{csch}\left(\sqrt{\epsilon_1}(\eta + cx + \mathrm{d}y + \omega t)\right).e^{i(cx+\mathrm{d}y+\omega t)}.\end{aligned} \tag{40}$$

Family 2: For constants f_1 and f_2, let $\epsilon_0 = 0$, $\epsilon_1 > 0$, and $\epsilon_2 = +4f_1f_2$;

$$\begin{aligned}W_3(x,y,t) =& \left(\pm\sqrt{-\frac{ab\epsilon_2\omega}{abc\epsilon_1\lambda_2 - c^2d\lambda_2}}\right)\\ & \frac{4f_1\sqrt{\epsilon_1}}{\left(4f_1^2 - \epsilon_2\right)\sinh\left(\sqrt{\epsilon_1}(\eta+\tau)\right) + \left(4f_1^2 - \epsilon_2\right)\cosh\left(\sqrt{\epsilon_1}(\eta+\tau)\right)}\\ & .e^{i(cx+\mathrm{d}y+\omega t)}.\end{aligned} \tag{41}$$

Family 3: For constants $R_1$and R_2, let $\epsilon_0 = \frac{\epsilon_1^2}{4\epsilon_2}$, $\epsilon_1 < 0$, and $\epsilon_2 > 0$;

$$\begin{aligned}W_4(x,y,t) =& \left(\pm\sqrt{-\frac{ab\epsilon_2\omega}{abc\epsilon_1\lambda_2 - c^2d\lambda_2}}\right)\sqrt{-\frac{\epsilon_1}{2\epsilon_2}}\\ & \tanh\left(\sqrt{-\frac{\epsilon_1}{2}}(\eta + cx + \mathrm{d}y + \omega t)\right).e^{i(cx+\mathrm{d}y+\omega t)},\end{aligned} \tag{42}$$

$$\begin{aligned}W_5(x,y,t) =& \left(\pm\sqrt{-\frac{ab\epsilon_2\omega}{abc\epsilon_1\lambda_2 - c^2d\lambda_2}}\right)\sqrt{-\frac{\epsilon_1}{2\epsilon_2}}\\ & \coth\left(\sqrt{-\frac{\epsilon_1}{2}}(\eta + cx + \mathrm{d}y + \omega t)\right).e^{i(cx+\mathrm{d}y+\omega t)}.\end{aligned} \tag{43}$$

For constants R_1 and R_2, let $\epsilon_0 = \frac{\epsilon_1^2}{4\epsilon_2}$, $\epsilon_1 < 0$, and $\epsilon_2 > 0$; then

$$W_6(x,y,t) = \left(\pm\sqrt{-\frac{ab\epsilon_2\omega}{abc\epsilon_1\lambda_2 - c^2d\lambda_2}}\right)\sqrt{-\frac{\epsilon_1}{2\epsilon_2}} \left(\tanh\left(\sqrt{-\frac{\epsilon_1}{2}}(\eta + cx + \mathrm{d}y + \omega t)\right)\right) + \operatorname{sech}\left(\sqrt{-2\epsilon_1}(\eta + cx + \mathrm{d}y + \omega t)\right)\Big).e^{i(cx+\mathrm{d}y+\omega t)}. \tag{44}$$

For constants R_1 and R_2, let $\epsilon_0 = \frac{\epsilon_1^2}{4\epsilon_2}$, $\epsilon_1 < 0$, and $\epsilon_2 > 0$; then

$$W_7(x,y,t) = \left(\pm\sqrt{-\frac{ab\epsilon_2\omega}{abc\epsilon_1\lambda_2 - c^2d\lambda_2}}\right)\sqrt{-\frac{\epsilon_1}{8\epsilon_2}} \left(\tanh\left(\sqrt{-\frac{\epsilon_1}{8}}(\eta + cx + \mathrm{d}y + \omega t)\right)\right) + \coth\left(\sqrt{-\frac{\epsilon_1}{8}}(\eta + cx + \mathrm{d}y + \omega t)\right).e^{i(cx+\mathrm{d}y+\omega t)}. \tag{45}$$

For constants R_1 and R_2, let $\epsilon_0 = \frac{\epsilon_1^2}{4\epsilon_2}$, $\epsilon_1 < 0$, and $\epsilon_2 > 0$; then

$$W_8(x,y,t) = \left(\pm\sqrt{-\frac{ab\epsilon_2\omega}{abc\epsilon_1\lambda_2 - c^2d\lambda_2}}\right) \frac{\sqrt{-\frac{\epsilon_1}{2\epsilon_2}}\cosh\left(\sqrt{-2\epsilon_1}(\eta + cx + \mathrm{d}y + \omega t)\right)}{\sinh\left(\sqrt{-2\epsilon_1}(\eta + cx + \mathrm{d}y + \omega t)\right) + i}. e^{i(cx+\mathrm{d}y+\omega t)}. \tag{46}$$

Family 4: Let $\epsilon_0 = 0$, $\epsilon_1 < 0$, and $\epsilon_2 \neq 0$; then

$$W_9(x,y,t) = \left(\pm\sqrt{-\frac{ab\epsilon_2\omega}{abc\epsilon_1\lambda_2 - c^2d\lambda_2}}\right)\sqrt{-\frac{\epsilon_1}{\epsilon_2}} \sec\left(\sqrt{-\epsilon_1}(\eta + cx + \mathrm{d}y + \omega t)\right).e^{i(cx+\mathrm{d}y+\omega t)}. \tag{47}$$

Let $\epsilon_0 = 0$, $\epsilon_1 < 0$, and $\epsilon_2 \neq 0$; then

$$W_{10}(x,y,t) = \left(\pm\sqrt{-\frac{ab\epsilon_2\omega}{abc\epsilon_1\lambda_2 - c^2d\lambda_2}}\right)\sqrt{-\frac{\epsilon_1}{\epsilon_2}} \csc\left(\sqrt{-\epsilon_1}(\eta + cx + \mathrm{d}y + \omega t)\right).e^{i(cx+\mathrm{d}y+\omega t)}. \tag{48}$$

Family 5: If $\epsilon_0 = \frac{\epsilon_1^2}{4\epsilon_2}$, $\epsilon_1 > 0$, $\epsilon_2 > 0$, and $R_1^2 - R_2^2 > 0$; then

$$W_{11}(x,y,t) = \left(\pm\sqrt{-\frac{ab\epsilon_2\omega}{abc\epsilon_1\lambda_2 - c^2d\lambda_2}}\right)\sqrt{-\frac{\epsilon_1}{2\epsilon_2}} \tan\left(\sqrt{\frac{\epsilon_1}{2}}(\eta + cx + \mathrm{d}y + \omega t)\right).e^{i(cx+\mathrm{d}y+\omega t)}. \tag{49}$$

If $\epsilon_0 = \frac{\epsilon_1^2}{4\epsilon_2}$, $\epsilon_1 > 0$, $\epsilon_2 > 0$, and $R_1^2 - R_2^2 > 0$; then

$$W_{12}(x,y,t) = \left(\pm\sqrt{-\frac{ab\epsilon_2\omega}{abc\epsilon_1\lambda_2 - c^2d\lambda_2}}\right) - \sqrt{-\frac{\epsilon_1}{2\epsilon_2}} \cot\left(\sqrt{\frac{\epsilon_1}{2}}(\eta + cx + \mathrm{d}y + \omega t)\right).e^{i(cx+\mathrm{d}y+\omega t)}. \tag{50}$$

Let $\epsilon_0 = \frac{\epsilon_1^2}{4\epsilon_2}$, $\epsilon_1 > 0$, $\epsilon_2 > 0$, and $R_1^2 - R_2^2 > 0$; then

$$W_{13}(x,y,t) = \left(\pm\sqrt{-\frac{ab\epsilon_2\omega}{abc\epsilon_1\lambda_2 - c^2d\lambda_2}}\right) - \sqrt{-\frac{\epsilon_1}{2\epsilon_2}}\Big(\tan\left(\sqrt{2\epsilon_1}(\eta + cx + \mathrm{d}y + \omega t)\right) - \sec\left(\sqrt{2\epsilon_1}(\eta + cx + \mathrm{d}y + \omega t)\right)\Big).e^{i(cx+\mathrm{d}y+\omega t)}. \tag{51}$$

Let $\epsilon_0 = \frac{\epsilon_1^2}{4\epsilon_2}$, $\epsilon_1 > 0$, $\epsilon_2 > 0$, and $R_1^2 - R_2^2 > 0$; then

$$W_{14}(x,y,t) = \left(\pm\sqrt{-\frac{ab\epsilon_2\omega}{abc\epsilon_1\lambda_2 - c^2d\lambda_2}}\right) \sqrt{-\frac{\epsilon_1}{8\epsilon_2}}\Big(\tan\Big(\sqrt{\frac{\epsilon_1}{8}}(\eta + cx + \mathrm{d}y + \omega t)\Big) - \cot\Big(\sqrt{\frac{\epsilon_1}{8}}(\eta + cx + \mathrm{d}y + \omega t)\Big)\Big).e^{i(cx+\mathrm{d}y+\omega t)}. \tag{52}$$

Let $\epsilon_0 = \frac{\epsilon_1^2}{4\epsilon_2}$, $\epsilon_1 > 0$, $\epsilon_2 > 0$, and $R_1^2 - R_2^2 > 0$; then

$$W_{15}(x,y,t) = \left(\pm\sqrt{-\frac{ab\epsilon_2\omega}{abc\epsilon_1\lambda_2 - c^2d\lambda_2}}\right) \frac{\sqrt{-\frac{\epsilon_1}{2\epsilon_2}}\left(\sqrt{R_1^2 - R_2^2 - W_1\cos\left(\sqrt{2\epsilon_1}(\eta + cx + \mathrm{d}y + \omega t)\right)}\right)}{\left(R_2 + W_1\sin\left(\sqrt{2\epsilon_1}(\eta + cx + \mathrm{d}y + \omega t)\right)\right)} .e^{i(cx+\mathrm{d}y+\omega t)},$$

$$W_{16}(x,y,t) = \left(\pm\sqrt{-\frac{ab\epsilon_2\omega}{abc\epsilon_1\lambda_2 - c^2d\lambda_2}}\right) \frac{\sqrt{-\frac{\epsilon_1}{2\epsilon_2}}\cos\left(\sqrt{2\epsilon_1}(\eta + cx + \mathrm{d}y + \omega t)\right)}{\sin\left(\sqrt{2\epsilon_1}(\eta + cx + \mathrm{d}y + \omega t)\right) - 1} .e^{i(cx+\mathrm{d}y+\omega t)}. \tag{53}$$

Family 6: Let $\epsilon_0 = 0$ and $\epsilon_1 > 0$; then

$$W_{17}(x,y,t) = \left(\pm\sqrt{-\frac{ab\epsilon_2\omega}{abc\epsilon_1\lambda_2 - c^2d\lambda_2}}\right) \frac{4\epsilon_1 e^{\sqrt{\epsilon_1}(\eta+cx+\mathrm{d}y+\omega t)}}{e^{2\sqrt{\epsilon_1}(\eta+cx+\mathrm{d}y+\omega t)} - 4\epsilon_1\epsilon_2}.e^{i(cx+\mathrm{d}y+\omega t)}. \tag{54}$$

Let $\epsilon_0 = 0$ and $\epsilon_1 > 0$; then

$$W_{18}(x,y,t) = \left(\pm\sqrt{-\frac{ab\epsilon_2\omega}{abc\epsilon_1\lambda_2 - c^2d\lambda_2}}\right) \frac{4\epsilon_1 e^{\sqrt{\epsilon_1}(\eta+cx+\mathrm{d}y+\omega t)}}{1 - 4\epsilon_1\epsilon_2 e^{2\sqrt{\epsilon_1}(\eta+cx+\mathrm{d}y+\omega t)}}.e^{i(cx+\mathrm{d}y+\omega t)}. \tag{55}$$

Family 7: Let $\epsilon_0 = 0$, $\epsilon_1 = 0$, and $\epsilon_2 > 0$; then

$$W_{19}(x,y,t) = \left(\pm\sqrt{-\frac{ab\epsilon_2\omega}{abc\epsilon_1\lambda_2 - c^2d\lambda_2}}\right) \frac{1}{\sqrt{\epsilon_2(\eta + cx + \mathrm{d}y + \omega t)}}.e^{i(cx+\mathrm{d}y+\omega t)}. \tag{56}$$

Let $\epsilon_0 = 0$, $\epsilon_1 = 0$, and $\epsilon_2 > 0$; then

$$W_{20}(x,y,t) = \left(\pm\sqrt{-\frac{ab\epsilon_2\omega}{abc\epsilon_1\lambda_2 - c^2d\lambda_2}}\right) \frac{i}{\sqrt{\epsilon_2(\eta + cx + \mathrm{d}y + \omega t)}}.e^{i(cx+\mathrm{d}y+\omega t)}. \tag{57}$$

3.1.1 Visual representation of KMN model via MSSE method

3.2 Modified auxiliary equation method

By using the homogeneous balancing algorithm, we find out the value of $M = 1$ as per the proposed method.

$$\begin{aligned}\mathcal{U}(\tau) &= m_0 + \sum_{i=1}^{n}\left(m_i(Q^f)^i + n_i(Q^f)^{-i}\right)\\ &= m_0 + m_1Q^f + n_1Q^{-f},\end{aligned} \tag{58}$$

where m_0, m_1, and n_1 are constants that are determined later. Substituting Eq. (58) together with Eq. (28) into Eq. (35), then set the coefficients of different powers of $k^{f(\tau)}$) to zero gives a system of algebraic equations, and solving them, we find out the following solutions.

$$\begin{aligned} m_0 &= \frac{\pm\frac{1}{2}\beta_2\sqrt{2}\sqrt{cd\lambda_1+\omega}}{\sqrt{\mathrm{c}}\sqrt{\lambda_2}\sqrt{4\alpha_1\sigma_1-\beta_2^2}},\\ m_1 &= \frac{\pm\sqrt{2}\sqrt{cd\lambda_1+\omega}\,\sigma_1}{\sqrt{\mathrm{c}}\sqrt{\lambda_2}\sqrt{4\alpha_1\sigma_1-\beta_2^2}}, n_1 = 0, a = \frac{2\left(cd\lambda_1+\omega\right)}{\left(4\alpha_1\sigma_1-\beta_2^2\right)a\lambda_1}.\end{aligned} \tag{59}$$

Family 1: If $\beta_1^2 - 4\sigma_1\alpha_1 < 0$ and $\sigma_1 \neq 0$,

$$\mathcal{U}_1(\tau) = \frac{\pm\frac{1}{2}\beta_2\sqrt{2}\sqrt{cd\lambda_1+\omega}}{\sqrt{\mathrm{c}}\sqrt{\lambda_2}\sqrt{4\alpha_1\sigma_1-\beta_2^2}} + \left(\frac{\pm\sqrt{2}\sqrt{cd\lambda_1+\omega}\,\sigma_1}{\sqrt{\mathrm{c}}\sqrt{\lambda_2}\sqrt{4\alpha_1\sigma_1-\beta_2^2}}\right) \left(\frac{-\beta_1 + \sqrt{4\sigma_1\alpha_1-\beta_1^2}\tan\left(\frac{\sqrt{4\sigma_1\alpha_1-\beta_1^2}\,\tau}{2}\right)}{2\sigma_1}\right). \tag{60}$$

$$\mathcal{U}_2(\tau) = \frac{\pm\frac{1}{2}\beta_2\sqrt{2}\sqrt{cd\lambda_1+\omega}}{\sqrt{\mathrm{c}}\sqrt{\lambda_2}\sqrt{4\alpha_1\sigma_1-\beta_2^2}} + \left(\frac{\pm\sqrt{2}\sqrt{cd\lambda_1+\omega}\,\sigma_1}{\sqrt{\mathrm{c}}\sqrt{\lambda_2}\sqrt{4\alpha_1\sigma_1-\beta_2^2}}\right) \left(\frac{-\beta_1 + \sqrt{4\sigma_1\alpha_1-\beta_1^2}\cot\left(\frac{\sqrt{4\sigma_1\alpha_1-\beta_1^2}\,\tau}{2}\right)}{2\sigma_1}\right). \tag{61}$$

Family 2: If $\beta_1^2 - 4\sigma_1\alpha_1 > 0$ and $\sigma_1 \neq 0$,

$$\mathcal{U}_3(\tau) = \frac{\pm\frac{1}{2}\beta_2\sqrt{2}\sqrt{cd\lambda_1+\omega}}{\sqrt{\mathrm{c}}\sqrt{\lambda_2}\sqrt{4\alpha_1\sigma_1-\beta_2^2}} + \left(\frac{\pm\sqrt{2}\sqrt{cd\lambda_1+\omega}\,\sigma_1}{\sqrt{\mathrm{c}}\sqrt{\lambda_2}\sqrt{4\alpha_1\sigma_1-\beta_2^2}}\right) \left(\frac{-\beta_1 + \sqrt{\beta_1^2-4\sigma_1\alpha_1}\tanh\left(\frac{\sqrt{\beta_1^2-4\sigma_1\alpha_1}\,\tau}{2}\right)}{2\sigma_1}\right). \tag{62}$$

$$\mathcal{U}_4(\tau) = \frac{\pm\frac{1}{2}\beta_2\sqrt{2}\sqrt{cd\lambda_1+\omega}}{\sqrt{\mathrm{c}}\sqrt{\lambda_2}\sqrt{4\alpha_1\sigma_1-\beta_2^2}} + \left(\frac{\pm\sqrt{2}\sqrt{cd\lambda_1+\omega}\,\sigma_1}{\sqrt{\mathrm{c}}\sqrt{\lambda_2}\sqrt{4\alpha_1\sigma_1-\beta_2^2}}\right) \left(\frac{-\beta_1 + \sqrt{\beta_1^2-4\sigma_1\alpha_1}\coth\left(\frac{\sqrt{\beta_1^2-4\sigma_1\alpha_1}\,\tau}{2}\right)}{2\sigma_1}\right). \tag{63}$$

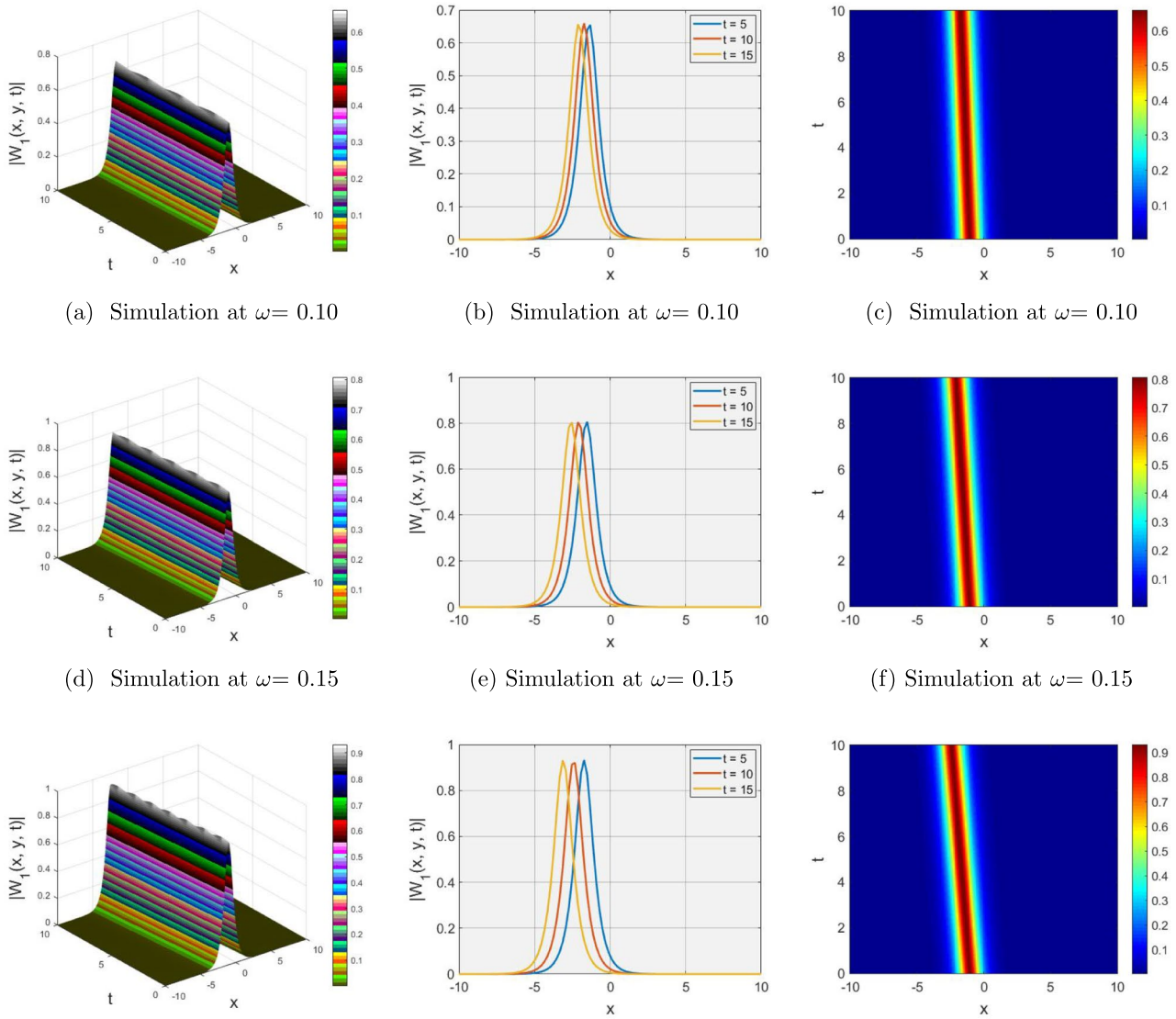

(a) Simulation at $\omega = 0.10$ (b) Simulation at $\omega = 0.10$ (c) Simulation at $\omega = 0.10$

(d) Simulation at $\omega = 0.15$ (e) Simulation at $\omega = 0.15$ (f) Simulation at $\omega = 0.15$

(g) Simulation at $\omega = 0.20$ (h) Simulation at $\omega = 0.20$ (i) Simulation at $\omega = 0.20$

Fig. 1 3D, density, and 2D visualization of the bright soliton solution of Eq. (39) with parameters $\lambda_1 = 0.5$, $a = 0.5$, $b = 1.25$, $\epsilon_1 = 1.6$, $\epsilon_2 = 0.8$, $c = 1.45$, $d = 0.75$, $\lambda_2 = 1.45$, and $\eta = 1.5$

Family 3: If $\beta_1^2 - 4\sigma_1\alpha_1 = 0$,

$$\mathcal{U}_5(\tau) = \frac{\pm\frac{1}{2}\beta_2\sqrt{2}\sqrt{cd\lambda_1 + \omega}}{\sqrt{c}\sqrt{\lambda_2}\sqrt{4\alpha_1\sigma_1 - \beta_2^2}} + \left(\frac{\pm\sqrt{2}\sqrt{cd\lambda_1 + \omega}\,\sigma_1}{\sqrt{c}\sqrt{\lambda_2}\sqrt{4\alpha_1\sigma_1 - \beta_2^2}}\right) \left(\frac{-2 + \beta_1\tau}{2\sigma_1\tau}\right). \tag{64}$$

3.2.1 Visualization of KMN model via MAE method

4 Results and discussion

The obtained wave solutions are visualized in the form of 3D, 2D, and density plots in order to demonstrate the dynamical properties of the KMN model. By varying parameter values, distinct types of soliton structures such as bright,

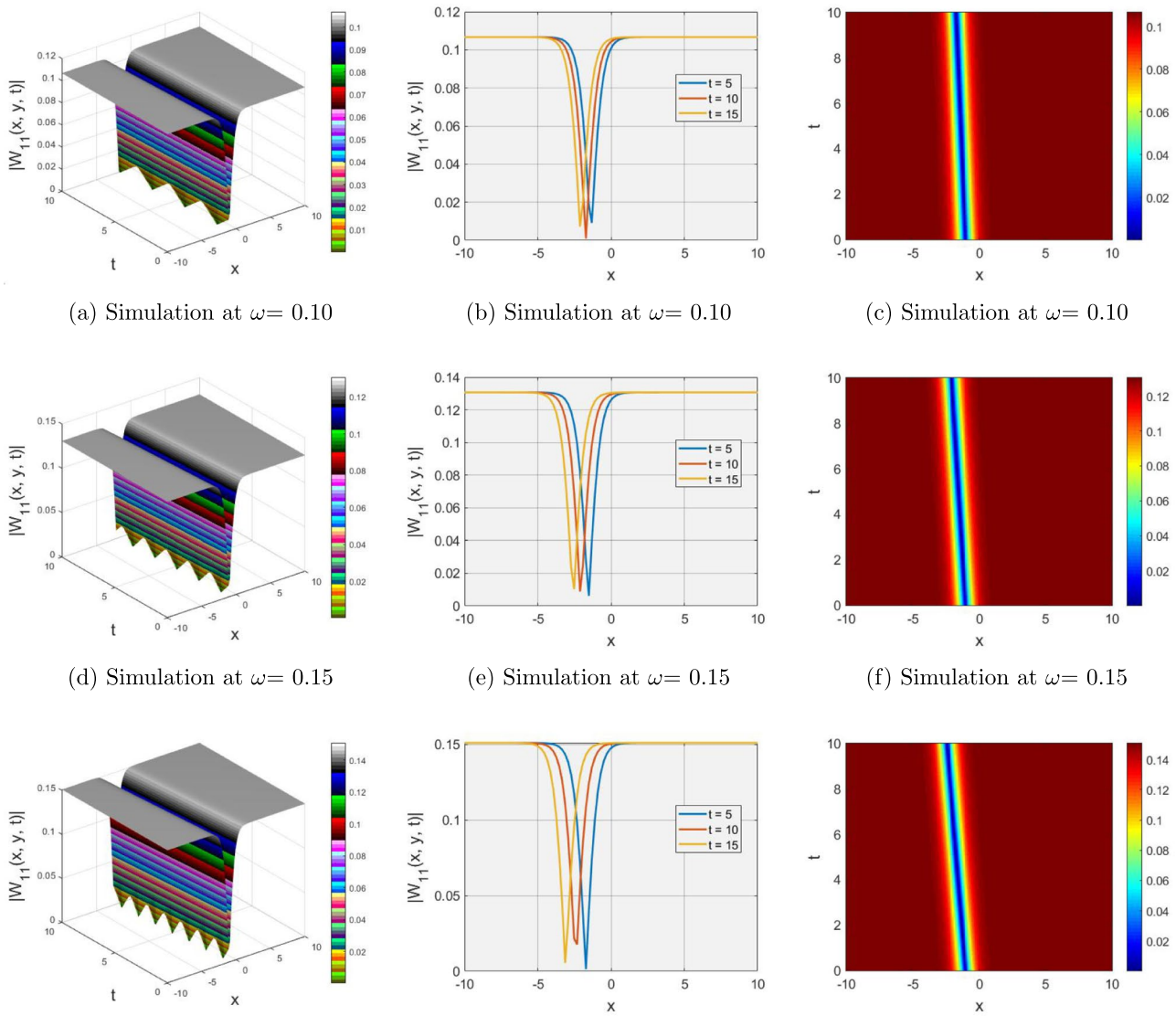

(a) Simulation at ω= 0.10 (b) Simulation at ω= 0.10 (c) Simulation at ω= 0.10

(d) Simulation at ω= 0.15 (e) Simulation at ω= 0.15 (f) Simulation at ω= 0.15

(g) Simulation at ω= 0.20 (h) Simulation at ω= 0.20 (i) Simulation at ω= 0.20

Fig. 2 3D, density, and 2D visualization of the dark soliton solution of Eq. (49) with parameters $\lambda_1 = 0.5$, $a = 0.5$, $b = 1.25$, $\epsilon_1 = -1.6$, $\epsilon_2 = 0.8$, $c = 1.45$, $d = 0.75$, $\lambda_2 = 1.45$, and $\eta = 1.5$

dark, singular, kink, and anti-kink solitons are observed. These results highlight the strong influence of nonlinear and dispersive parameters on the morphology and propagation of solitary waves. Graphical representations help illustrate the amplitude, profile, and evolution of the solutions, offering a clearer physical interpretation of the system.

Figures 1, 2, 3 present the wave solutions generated using the MSSE method. In Fig. 1, the solution $W_1(x, y, t)$ corresponds to a bright soliton, displayed in 3D, 2D, and density forms, with parameter values $\lambda_1 = 0.5$, $a = 0.5$, $b = 1.25$, $\epsilon_1 = 1.6$, $\epsilon_2 = 0.8$, $c = 1.45$, $d = 0.75$, $\lambda_2 = 1.45$, and $\eta = 1.5$. When the nonlinear coefficient is modified from $\epsilon_1 = 1.6$ to $\epsilon_1 = -1.6$ (while keeping all other parameters fixed), the wave solution transforms into a dark soliton, denoted $W_{11}(x, y, t)$, which is also displayed in Fig. 2. This highlights that the sign of ϵ_1 determines the bright or dark nature of the soliton. Furthermore, a singular soliton solution $W_{15}(x, y, t)$ is obtained when the parameters are set to $\lambda_1 = 0.25$, $\lambda_2 = 1.15$, $a = 0.5$, $b = -0.25$, $c = 1.25$, $\epsilon_1 = -0.45$, $\epsilon_2 = 1.5$, $R_1 = -1.35$, $R_2 = 5.45$, $W_1 = 0.5$, and $\eta = 0.5$, as visualized in Fig. 3.

Figures 4, 5, 6 display the wave solutions constructed using the MAE method. In Fig. 4, the solution $U_1(\tau)$ simulates an anti-kink soliton with parameter values $\lambda_1 = 1.25$, $\lambda_2 = 1.15$, $a = 1.5$, $b = 1.25$, $c = 2.9$, $d = 1.5$, $\epsilon_1 = 1.45$, $\epsilon_2 = 0.45$, $\beta_1 = 1.8$, $\beta_2 = 0.2$, $\alpha_1 = 1.5$, $\alpha_2 = 1.5$, $\sigma_1 = 10.5$,

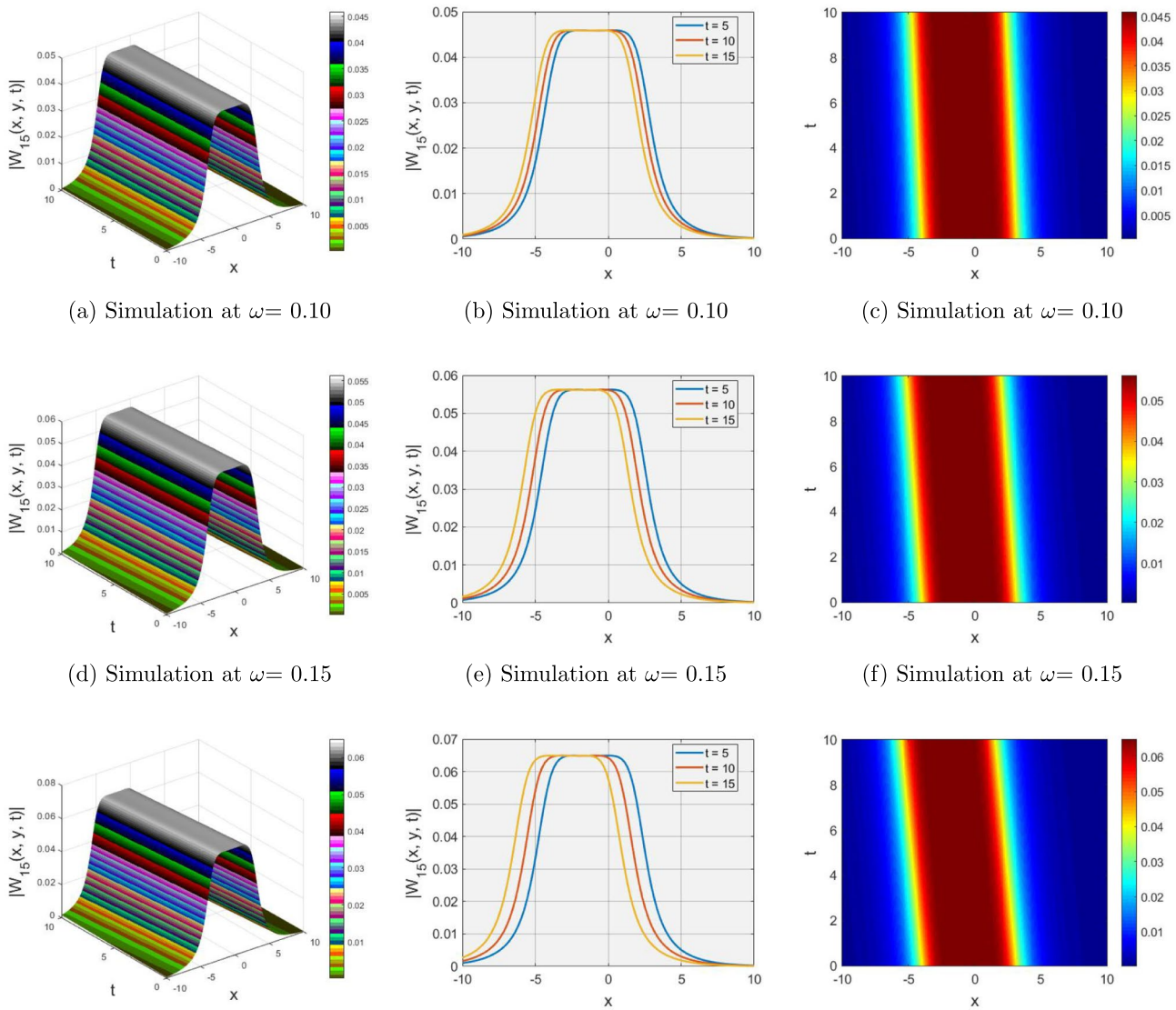

(a) Simulation at ω= 0.10 (b) Simulation at ω= 0.10 (c) Simulation at ω= 0.10

(d) Simulation at ω= 0.15 (e) Simulation at ω= 0.15 (f) Simulation at ω= 0.15

(g) Simulation at ω= 0.20 (h) Simulation at ω= 0.20 (i) Simulation at ω= 0.20

Fig. 3 3D, density, and 2D visualization of the singular soliton of Eq. (53) with parameters $\lambda_1 = 0.25$, $\lambda_2 = 1.15$, $a = 0.5$, $b = -0.25$, $c = 1.25$, $\epsilon_1 = -0.45$, $\epsilon_2 = 1.5$, $R_1 = -1.35$, $R_2 = 5.45$, $W_1 = 0.5$, and $\eta = 0.5$

and $\eta = 0.5$. Figure 5 shows the solution $U_2(\tau)$, which reveals a periodic soliton structure for $\lambda_1 = 0.25$, $\lambda_2 = 0.15$, $a = 0.5$, $b = 0.25$, $c = 1.0$, $d = 0.5$, $\epsilon_1 = 0.45$, $\epsilon_2 = 0.5$, $\beta_1 = 0.8$, $\beta_2 = 2.2$, $\alpha_1 = 2.5$, $\alpha_2 = 2.5$, $\sigma_1 = 2.5$, and $\eta = -1.5$. Finally, Fig. 6 depicts the solution $U_3(\tau)$, which corresponds to a kink soliton, obtained with parameter values $\lambda_1 = 0.25$, $\lambda_2 = 0.15$, $a = 0.5$, $b = 0.25$, $c = -1.0$, $d = 0.5$, $\epsilon_1 = 0.45$, $\epsilon_2 = 0.5$, $\beta_1 = 0.8$, $\beta_2 = 2.2$, $\alpha_1 = 2.5$, $\alpha_2 = 2.5$, $\sigma_1 = 2.5$, and $\eta = -1.5$. Dispersion parameters (λ_1, λ_2) and auxiliary constants ($R_1, W_1, \beta_1, \alpha_1, \sigma_1$) were kept in moderate ranges (0.15–1.50 and model-consistent values) to ensure soliton stability. Nonlinearity (ϵ_1, ϵ_2, –1.6 to 1.6) and shape-control (a, b, c, d, η, –1.5 to 3.0) parameters were varied to capture both bright and dark soliton regimes.

These simulations confirm that the qualitative nature of the soliton solution strongly depends on the selection of parameters. Nonlinear coefficients (ϵ_1, ϵ_2) determine the transition between bright and dark solitons, while the signs and magnitudes of parameters such as c and η govern the emergence of kink, anti-kink, or periodic solitons. Dispersion-related parameters (λ_1, λ_2) also influence wave width and stability. The obtained results emphasize the delicate balance between nonlinearity and dispersion, which ensures that the soliton retains its localized profile while exhibiting

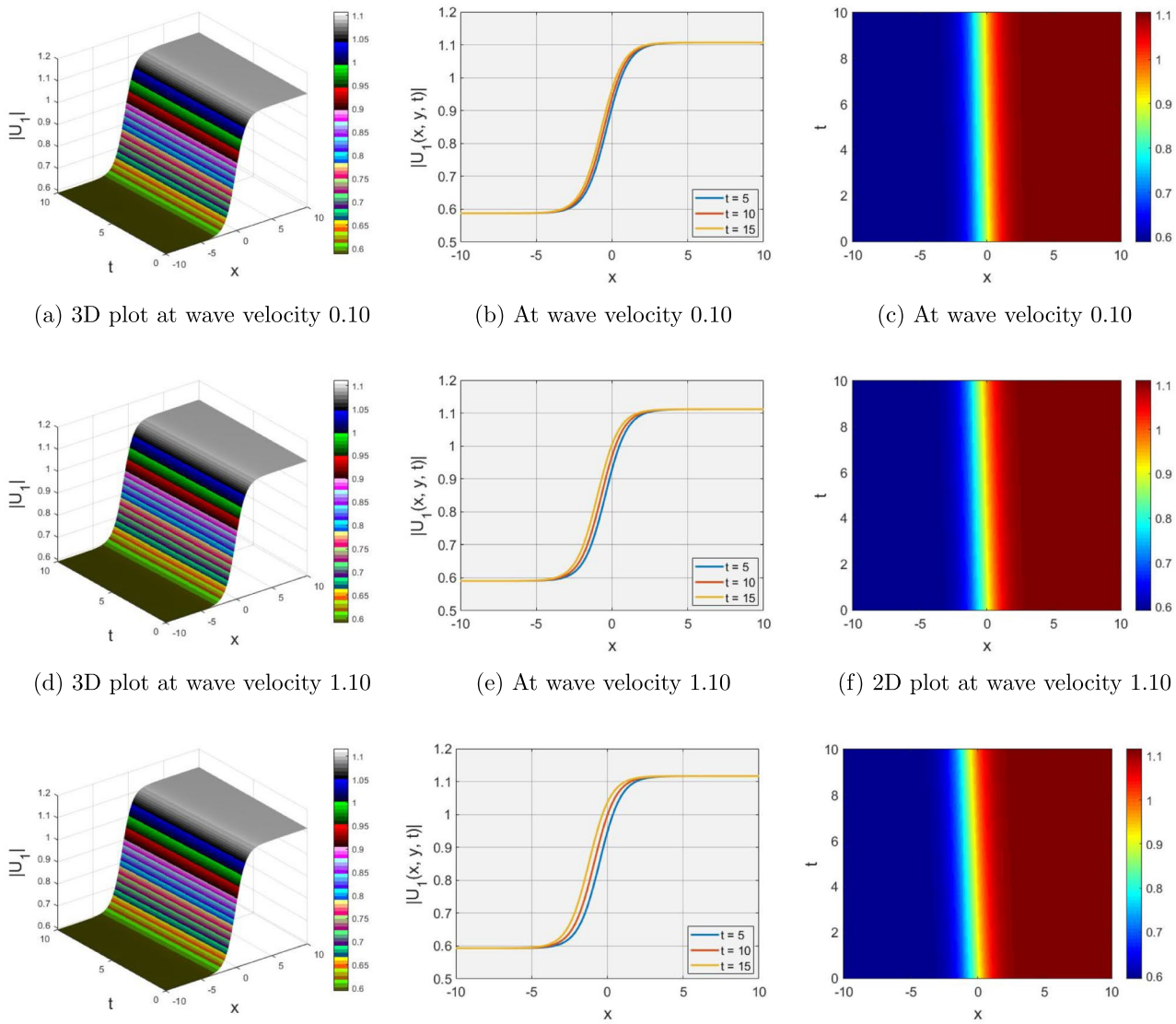

(a) 3D plot at wave velocity 0.10 (b) At wave velocity 0.10 (c) At wave velocity 0.10

(d) 3D plot at wave velocity 1.10 (e) At wave velocity 1.10 (f) 2D plot at wave velocity 1.10

(g) 3D plot at wave velocity 2.10 (h) Density plot at wave velocity 2.10 (i) 2D plot at wave velocity 2.10

Fig. 4 3D, density, and 2D visualization of the anti kink soliton solution of Eq. (60) with parameters $\lambda_1 = 1.25$, $\lambda_2 = 1.15$, $a = 1.5$, $b = 1.25$, $c = 2.9$, $d = 1.5$, $\epsilon_1 = 1.45$, $\epsilon_2 = 0.45$, $\beta_1 = 1.8$, $\beta_2 = 0.2$, $\alpha_1 = 1.5$, $\alpha_2 = 1.5$, $\sigma_1 = 10.5$, and $\eta = 0.5$

a variety of possible structures depending on parameter choice.

4.1 Physical implications

The KMN model provides a rich framework for understanding nonlinear wave dynamics in two-dimensional dispersive media, and its soliton solutions display distinct behaviors with important physical implications for optical fibers. The bright soliton maintains a localized peak of intensity as it propagates, its dynamics stabilized by the exact balance between anomalous dispersion and nonlinear self-focusing; in optical fibers operating near 1550 nm, this stability enables high-speed, long-distance data transmission with minimal distortion, making bright solitons central to soliton-based communication systems. In contrast, the dark soliton evolves as a localized intensity dip against a continuous background, with its motion governed by a phase gradient that induces velocity; dynamically, dark solitons are remarkably robust, surviving collisions and perturbations with little deformation, and in fiber systems, this robustness makes them valuable for coherent communication, phase-encoded transmission, and all-optical switching. The singular soliton behaves very differently: its dynamics involve finite-time blow-up, where energy focuses into an extremely localized region, mimicking collapse phenomena; in optics, such

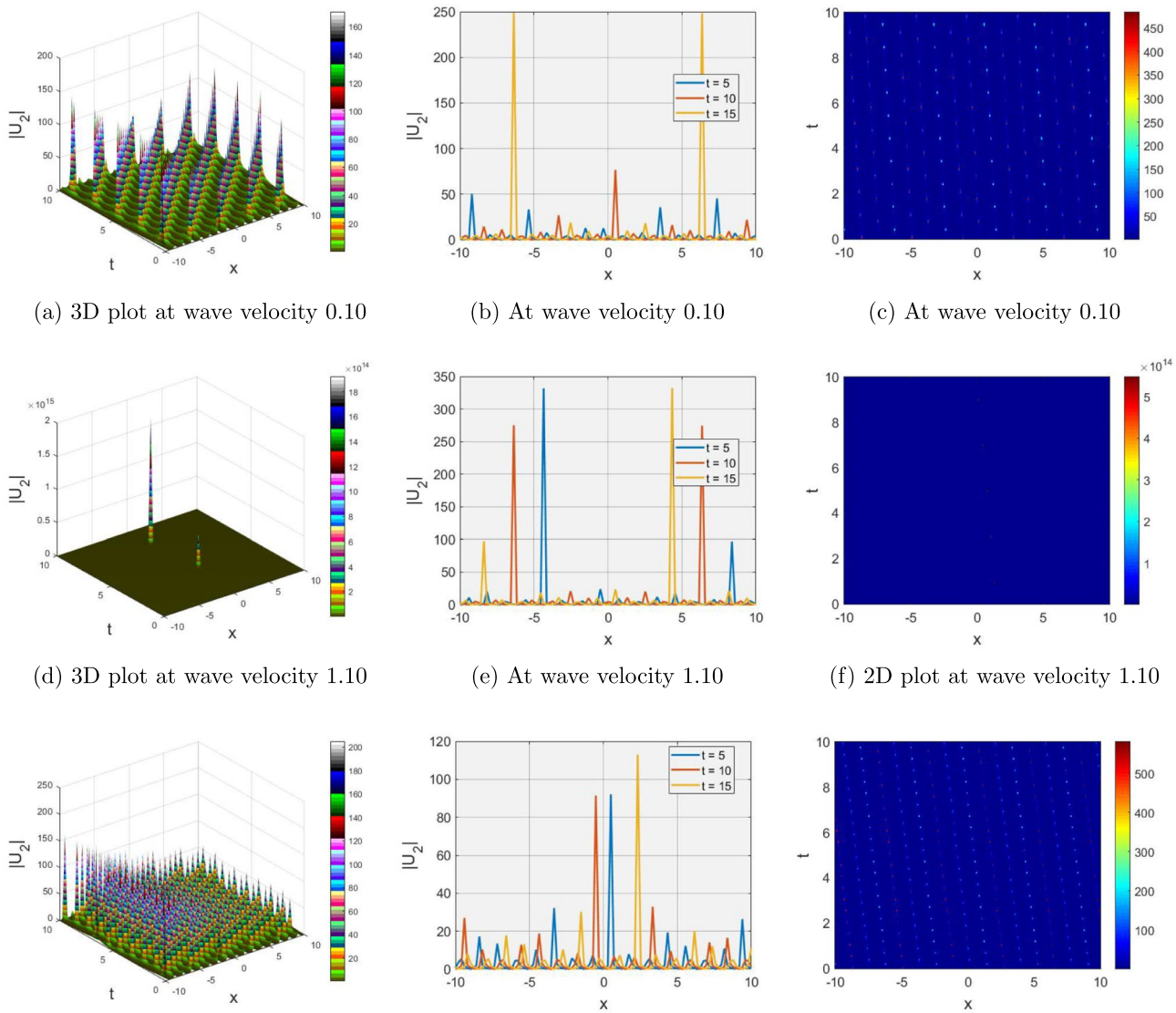

(a) 3D plot at wave velocity 0.10 (b) At wave velocity 0.10 (c) At wave velocity 0.10

(d) 3D plot at wave velocity 1.10 (e) At wave velocity 1.10 (f) 2D plot at wave velocity 1.10

(g) 3D plot at wave velocity 2.10 (h) Density plot at wave velocity 2.10 (i) 2D plot at wave velocity 2.10

Fig. 5 3D, density, and 2D visualization of the periodic soliton solution of Eq. (61) with parameters $\lambda_1 = 0.25$, $\lambda_2 = 0.15$, $a = 0.5$, $b = 0.25$, $c = 1.0$, $d = 0.5$, $\epsilon_1 = 0.45$, $\epsilon_2 = 0.5$, $\beta_1 = 0.8$, $\beta_2 = 2.2$, $\alpha_1 = 2.5$, $\alpha_2 = 2.5$, $\sigma_1 = 2.5$, and $\eta = -1.5$

behavior corresponds to rogue waves or catastrophic self-focusing in fibers, with implications for super continuum generation in photonic devices and for identifying thresholds of fiber damage at high power. The periodic soliton, which evolves as a repeating train of pulses described by elliptic functions, exhibits recurrence dynamics in which dispersion and nonlinearity exchange energy in a stable cycle; in practical terms, these dynamics underlie optical frequency combs and mode-locked fiber lasers, essential for precision metrology, spectroscopy, and dense wavelength-division multiplexing in communications. The kink soliton propagates as a nonlinear wavefront connecting two distinct background states, maintaining its step-like structure as it moves; such dynamics resemble domain-wall propagation and enable controlled intensity switching, which in fiber systems is harnessed for optical logic gates and bistable devices. Its counterpart, the anti kink soliton, describes the reverse transition, with mirror-like dynamics that support bidirectional switching; together, kink and anti kink solitons are central to reconfigurable optical circuits and optical memory technologies, where forward and backward transitions are both required. In summary, the KMN soliton solutions whether stable bright and dark pulses, collapsing singular structures, periodic trains, or topological kink fronts

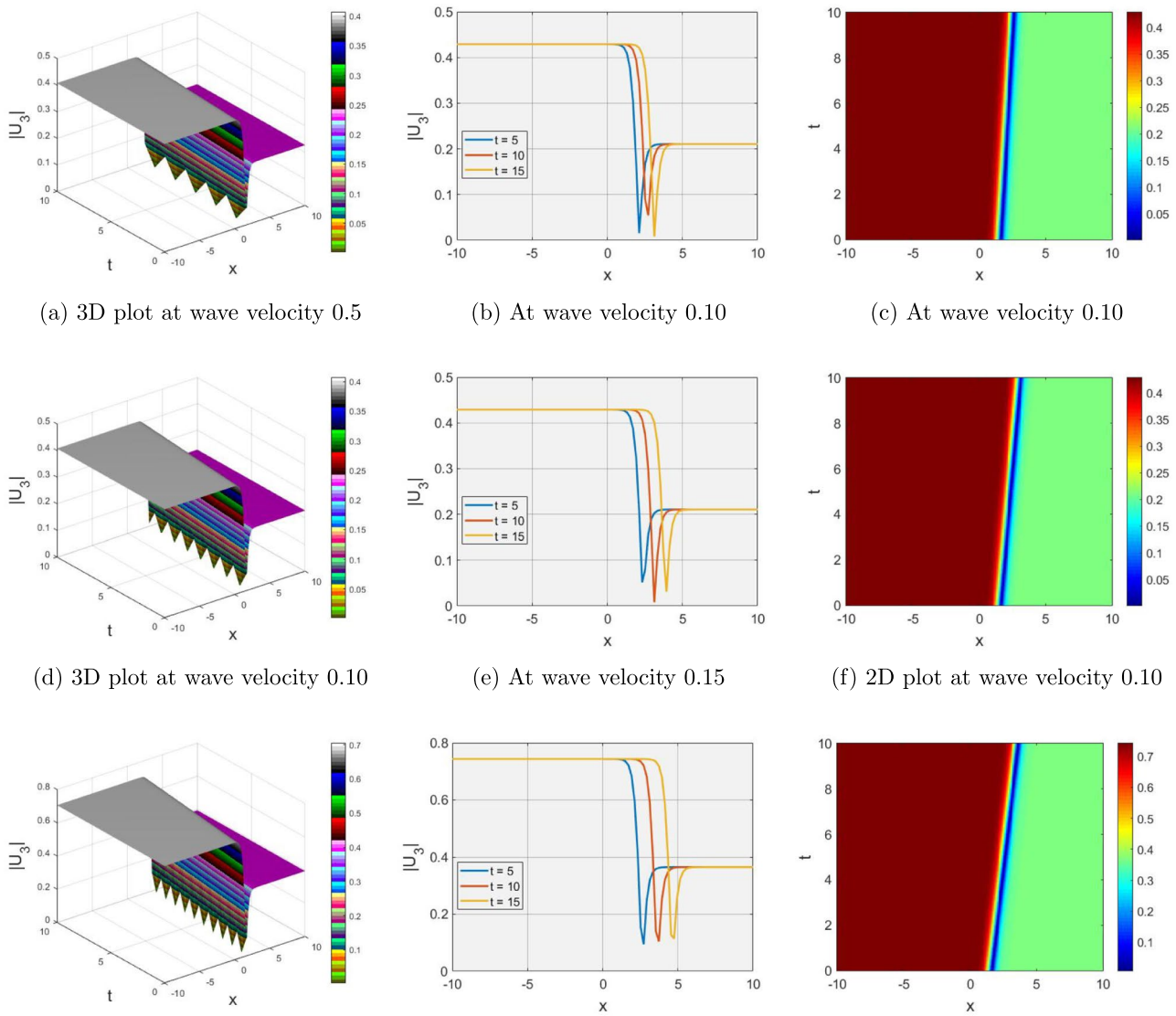

(a) 3D plot at wave velocity 0.5 (b) At wave velocity 0.10 (c) At wave velocity 0.10

(d) 3D plot at wave velocity 0.10 (e) At wave velocity 0.15 (f) 2D plot at wave velocity 0.10

(g) 3D plot at wave velocity 0.15 (h) Density plot at wave velocity 0.15 (i) 2D plot at wave velocity 0.15

Fig. 6 3D, density, and 2D visualization of the kink soliton solution of Eq. (62) with parameters $\lambda_1 = 0.25$, $\lambda_2 = 0.15$, $a = 0.5$, $b = 0.25$, $c = -1.0$, $d = 0.5$, $\epsilon_1 = 0.45$, $\epsilon_2 = 0.5$, $\beta_1 = 0.8$, $\beta_2 = 2.2$, $\alpha_1 = 2.5$, $\alpha_2 = 2.5$, $\sigma_1 = 2.5$, and $\eta = -1.5$

illustrate the diverse dynamical regimes supported by the balance of dispersion and nonlinearity, and their physical implications directly align with the practical needs of optical fiber systems for robust communication, switching, frequency control, and understanding of nonlinear instabilities.

5 Sensitivity analysis

First of all, by using the theory of planar dynamical systems, Eq. (35) is converted into the following dynamical system:

$$\begin{cases} \frac{d\mathcal{Y}}{d\vartheta} = M, \\ \frac{dM}{d\vartheta} = \left(\frac{w+\lambda_1 cd}{\lambda_1 ab}\right)\mathcal{Y} - \left(\frac{2c\lambda_2}{\lambda_1 ab}\right)\mathcal{Y}^3, \end{cases} \tag{65}$$

with parameters $w = 0.5$, $\lambda_1 = 0.4$, $c = 0.2$, $d = 0.4$, $a = 0.35$, $b = 0.12$, and $\lambda_2 = 0.45$. The objective is to conduct sensitivity analysis to see how the system reacts under different initial conditions. Figures 7a–7d depict the two solutions graphically for a variety of initial data. Figure 7a uses the initial conditions $(\mathcal{Y}, M) = (0.0, 0.05)$ in the red line and $(\mathcal{Y}, M) = (0.0, 1.01)$ in the blue line. In Fig. 7b,

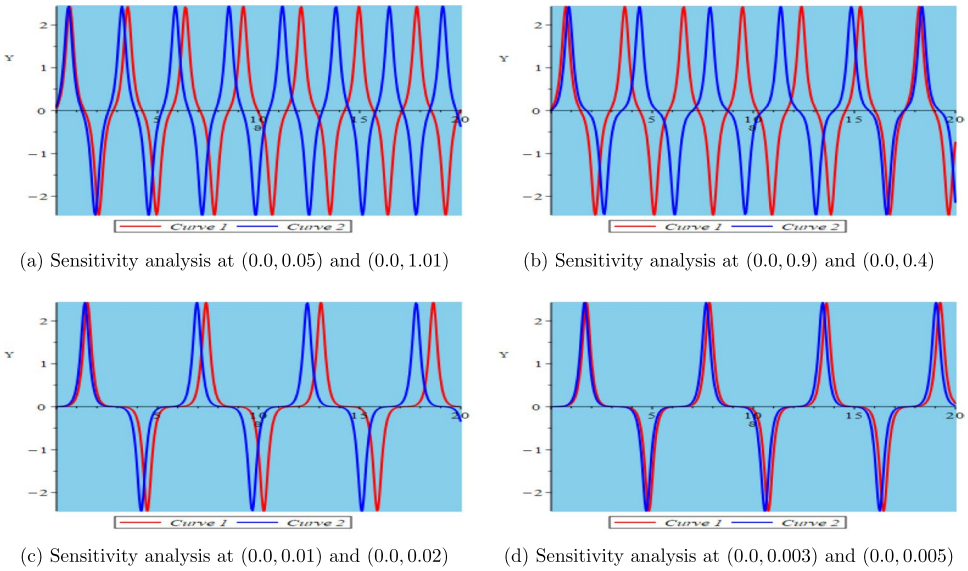

Fig. 7 Sensitivity demonstration of dynamical system (65) at various initial conditions

(a) Sensitivity analysis at $(0.0, 0.05)$ and $(0.0, 1.01)$

(b) Sensitivity analysis at $(0.0, 0.9)$ and $(0.0, 0.4)$

(c) Sensitivity analysis at $(0.0, 0.01)$ and $(0.0, 0.02)$

(d) Sensitivity analysis at $(0.0, 0.003)$ and $(0.0, 0.005)$

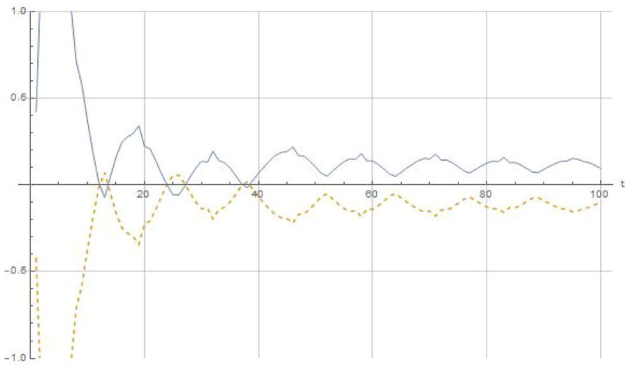

Fig. 8 Lyapunov plot for perturbed dynamical system (66)

the initial conditions $(\mathcal{Y}, M) = (0.0, 0.9)$ in the red line and $(\mathcal{Y}, M) = (0.0, 0.4)$ in the blue line are applied. In Fig. 7c, the initial conditions $(\mathcal{Y}, M) = (0.0, 0.01)$ in the red line and $(\mathcal{Y}, M) = (0.0, 0.02)$ in the blue line are applied. Figure 7d uses the initial conditions $(\mathcal{Y}, M) = (0.0, 0.003)$ in the red line and $(\mathcal{Y}, M) = (0.0, 0.005)$ in the blue line. Figure 7 demonstrates that small variations in initial conditions may lead to noticeably different solution trajectories, highlighting the sensitivity of the system.

The connection between these sensitivity results and soliton stability in practical applications is significant. In optical fiber systems and related nonlinear media, soliton-based transmission requires robustness to small fluctuations in initial pulse profiles or external perturbations. The sensitivity analysis shows that for certain parameter regimes, small changes in the initial state can lead to divergent solution paths, which would correspond to unstable soliton propagation in practice. Conversely, regimes where trajectories remain close despite perturbations reflect conditions under which soliton solutions are stable and physically realizable. Thus, sensitivity analysis not only characterizes the mathematical response of the system but also provides insight into the practical reliability of solitons in real-world applications such as fiber-optic communication, where initial condition perturbations and environmental noise are unavoidable.

5.1 Lyapunov exponents

To investigate the stability properties of the nonlinear system through Lyapunov exponents [52], we introduce a weak external periodic forcing into the model. Specifically, by adding the perturbation term $\sigma \cos(\omega\xi)$, the dynamical system Eq. (65) is modified as

$$\begin{cases} \frac{d\mathcal{Y}}{d\vartheta} = M, \\ \frac{dM}{d\vartheta} = (\frac{w+\lambda_1 cd}{\lambda_1 ab})\mathcal{Y} - (\frac{2c\lambda_2}{\lambda_1 ab})\mathcal{Y}^3 + cos(\omega\xi) \end{cases} \tag{66}$$

The stability of the nonlinear dynamical system was investigated through the computation of Lyapunov exponents using the variational equations method under the parameter set $w = 0.5$, $\lambda_1 = 0.4$, $c = 0.2$, $d = 0.4$, $a = 0.35$, $b = 0.12$, and $\lambda_2 = 0.45$ with perturbation amplitude $\sigma = 0.001$ and frequency $\omega = 3$. The results, shown in Fig. (8), reveal the evolution of the two Lyapunov exponents. Initially, the largest exponent is positive and the second exponent is strongly negative, reflecting transient dynamics. However, as time progresses beyond $t \approx 20$, the largest exponent fluctuates around zero while the second remains negative. This spectrum indicates that the system is non-chaotic, since no persistently positive Lyapunov exponent is observed. Dynamically, the negative exponent confirms contraction in one direction, leading to decay of perturbations, while the near-zero exponent suggests neutral stability in the other

Table 1 Comparison of our solutions by MSSE and MAE Techniques

Solutions obtained by MSSE method	Solutions obtained by MAE method
(i) Constructed the 20-wave solution with seven families using this effective method	(i) This method has five wave solutions with three families
(ii) In this method the solutions are represented in the form of trigonometric(sin, cos, tan, cot, sec), hyperbolic (sinh, cosh, tanh, coth, sech , csch), and rational functions	(ii) Provide the solutions in the form of trigonometric(tan, cot), hyperbolic (tanh, coth), and rational functions
(iii) This approach provides the optimal configurations of solitons, such as bright-shaped, dark-shaped, and singular soliton profiles.	(iii) This approach investigates solitons in the form of periodic, kink, and anti kink profile patterns.
(iv) The results of this study are more pertinent than those produced via the MAE technique	(iv) The application domains are extensive but not as comprehensive as the MSSE method
(v) This method works well for studying soliton wave solutions to the KMN model	(v) The method is also suitable for exploring the soliton wave solutions to KMN model

Table 2 Research Comparison of Existing and New Results

Existing research	Existing results	New results
Yıldırım [32]	singular periodic solitons	kink and anti kink solitons
Kumar et al. [35]	U shaped soliton	periodic, kink and anti kink
Jhangeer et al. [36]	dark, dark-bright, and dark singular	periodic, anti-kink, kink, and bright
Singh et al. [40]	bright-dark, complexiton	dark, anti-kink, kink, and bright
Rezazade et al. [42]	lump-soliton, rogue waves	singular, periodic, anti-kink, kink

direction, corresponding to quasi-periodic oscillations. Physically, this implies that the nonlinear waveforms governed by the KMN-type model remain stable under these parameter regimes, with soliton structures retaining their integrity against perturbations. The presence of a negative exponent supports the robustness of localized solitons, whereas the near-zero exponent reflects the persistence of recurrence phenomena such as periodic or kink solitons. This motivates the computation of Lyapunov exponents as a quantitative measure of sensitivity to initial conditions and as a diagnostic tool for identifying whether the perturbed system evolves toward stable, quasi-periodic, or chaotic regimes (Table 1).

5.2 Comparison with previous studies

The effectiveness of the MSSE and MAE methods is further demonstrated by comparing the obtained solutions with results available in the literature. Several researchers have explored the KMN model using diverse analytical techniques, and their findings provide a useful benchmark for evaluating the novelty of the present results. Yıldırım [32], by employing the modified simple equation method, reported dark, bright, and singular periodic solutions. Some of these solutions are consistent with those derived in this study, whereas others exhibit structural differences, as presented in Table 2. Kumar et al. [35] applied the generalized Kudryashov method and the new auxiliary equation method to generate dark, bright, periodic-shaped, and singular solitons. A number of their results overlap with ours, while certain distinctive features of our solutions set them apart. Jhangeer et al. [36] used the direct algebraic extension method to establish dark–bright, dark–singular, and purely singular solutions. In contrast, our approach succeeds in obtaining not only bright and dark solitons but also kink, anti-kink, and periodic solitons, thereby extending the solution space. Singh et al. [40] constructed bright–dark optical solitons, periodic waveforms, complexiton solutions, and rational structures, whereas Rezazade et al. [42] identified lump solitons and rogue wave phenomena.

The present study enriches the existing body of work by producing a broader class of soliton solutions that includes bright solitons, dark solitons, kink solitons, anti-kink solitons, and singular solitons through the MSSE and MAE frameworks. Unlike previous contributions, which were largely confined to bright–dark or singular categories, our results demonstrate the coexistence of multiple soliton families within the KMN model. This comprehensive spectrum of solutions underscores the novelty of the adopted methods and establishes new avenues for further physical and mathematical exploration of nonlinear wave phenomena. In addition, sensitivity analysis and Lyapunov exponent visualizations of the associated dynamical system were carried out under different initial conditions. Our method is more efficient, requiring less computational time while maintaining accuracy and stability across the chosen parameter ranges. These analyses provide both qualitative and quantitative insights into the behavior of the model and further demonstrate the originality and novelty of the present work.

6 Conclusion

This study investigated the KMN model and derived a variety of soliton solutions including bright, dark, W-shaped, combined bright–dark, and periodic solitons by employing the modified Sardar sub-equation method (MSSEM) and the modified auxiliary equation method (MAEM). The solutions were visualized through 2D, 3D profiles and density plots, revealing their structural characteristics under selected parameter values. These results have practical significance in optical fiber communications, telecommunications, fluid dynamics, and ocean engineering. Sensitivity analysis and Lyapunov exponent evaluation demonstrated that even small variations in initial conditions can markedly influence solution stability, indicating the model's strong parameter dependence. The Lyapunov exponent analysis further quantified the degree of stability or instability of the waveforms, with positive values indicating chaotic behavior and negative values reflecting stable dynamics. This combined approach provides a deeper understanding of the nonlinear characteristics of the KMN model, supporting its applicability in both theoretical and engineering contexts. Comparative analysis with existing results confirms the novelty and effectiveness of the proposed solutions.

Acknowledgment The authors extend their appreciation to the Deanship of Scientific Research and Graduate Studies at King Khalid University for funding this work through small Group Project under grant number (project number RGP1-265-45. Academic year 1445H) and aslo this article has been supported by EU funds under the project "Increasing the resilience of power grids in the context of decarbonisation, decentralisation and sustainable socioeconomic development", CZ.02.01.01/00/23_021/0008759, through the Operational Programme Johannes Amos Comenius.

Author Contributions All authors have contributed equally to this manuscript

Funding No funding has been received for this research.

Data Availability No datasets were generated or analyzed during the current study.

Declarations

Conflict of interest The authors declare no Conflict of interest.

References

1. R. Li, Z.A.B. Sinnah, Z.M. Shatouri, J. Manafian, M.F. Aghdaei, A. Kadi, Different forms of optical soliton solutions to the kudryashov's quintuple self-phase modulation with dual-form of generalized nonlocal nonlinearity. Results Phys. **46**, 106293 (2023)
2. Z. Li, C. Liu, Chaotic pattern and travelling wave solution of the perturbed stochastic nonlinear schrödinger equation with generalized anti-cubic law nonlinearity and spatio-temporal dispersion. Results Phys. **56**, 107305 (2024)
3. Z. Li, E. Hussain, Qualitative analysis and optical solitons for the (1+ 1)-dimensional biswas-milovic equation with parabolic law and nonlocal nonlinearity. Results Phys. **56**, 107304 (2024)
4. X. Liu, B. Abd Alreda, J. Manafian, B. Eslami, M.F. Aghdaei, M. Abotaleb, A. Kadi, Computational modeling of wave propagation in plasma physics over the gilson-pickering equation. Results Phys. **50**, 106579 (2023)
5. S.D. Yogita, H. Kumar, A. Kumar, M.S. Gautam, Part. Differ. Equ Appl. Math. **4**, 100136 (2021)
6. R. Li, J. Manafian, H.A. Lafta, H.A. Kareem, K.F. Uktamov, M. Abotaleb, The nonlinear vibration and dispersive wave systems with cross-kink and solitary wave solutions. Int. J. Geom. Methods Modern Phys. **19**(10), 2250151 (2022)
7. M. Alquran, Classification of single-wave and bi-wave motion through fourth-order equations generated from the ito model. Phys. Scr. **98**(8), 085207 (2023)
8. A.A. Sagher, M.I. Asjad, T. Muhammad, Advanced techniques for analyzing solitary waves in circular rods: a sensitivity visualization study. Opt. Quant. Electron. **56**(10), 1673 (2024)
9. Q.J. Feng, G.Q. Zhang, Lump solution, lump-stripe solution, rogue wave solution and periodic solution of the (2+ 1)-dimensional Fokas system. Nonlinear Dyn. 1-18 (2024)
10. N. Ahmed, M. Rani, S.S. Dragomir, B. Bin-Mohsin, Optical soliton solutions of Fokas system and (2+ 1) Davey-Stewartson system by mapping method. Physica Scripta (2024)
11. S. Tarla, K.K. Ali, T.C. Sun, R. Yilmazer, M.S. Osman, Nonlinear pulse propagation for novel optical solitons modeled by fokas system in monomode optical fibers. Results Phys. **36**, 105381 (2022)
12. K.J. Wang, J.H. Liu, J. Wu, Soliton solutions to the fokas system arising in monomode optical fibers. Optik **251**, 168319 (2022)
13. S.S. Atas, K.K. Ali, T.A. Sulaiman, H. Bulut, Optical solitons to the fokas system equation in monomode optical fibers. Opt. Quant. Electron. **54**(11), 707 (2022)
14. S. Kumar, A. Kumar, Newly generated optical wave solutions and dynamical behaviors of the highly nonlinear coupled Davey-Stewartson Fokas system in monomode optical fibers. Optical and Quantum Electronics, 55(6), 566. Quant. Electron. **55**(8), 723 (2023)
15. M.M. Khater, Nonlinear elastic circular rod with lateral inertia and finite radius: dynamical attributive of longitudinal oscillation. Int. J. Mod. Phys. B **37**(06), 2350052 (2023)
16. M.M. Khater, Physics of crystal lattices and plasma; analytical and numerical simulations of the gilson-pickering equation. Results Phys. **44**, 106193 (2023)
17. E.M. Zayed, K.A. Gepreel, R.M. Shohib, M.E. Alngar, Y. Yıldırım, Optical solitons for the perturbed biswas-milovic equation with kudryashov's law of refractive index by the unified auxiliary equation method. Optik **230**, 166286 (2021)
18. M. Khater, A. Jhangeer, H. Rezazadeh, L. Akinyemi, M.A. Akbar, M. Inc, H. Ahmad, New kinds of analytical solitary wave solutions for ionic currents on microtubules equation via two different techniques. Opt. Quant. Electron. **53**(11), 1–27 (2021)
19. M.M. Khater, Multi-vector with nonlocal and non-singular kernel ultrashort optical solitons pulses waves in birefringent fibers. Chaos Solit. Fract. **167**, 113098 (2023)
20. N.T. Alqurashi, M. Manzoor, S.Z. Majid, M.I. Asjad, M.S. Osman, Solitary waves pattern appear in tropical tropospheres and nonlinear landau–ginzburg–higgs equation mid-latitudes with chaotic analysis. Results Phys. **54**, 107116 (2023)
21. S.F. Tian, M.J. Xu, T.T. Zhang, A symmetry-preserving difference scheme and analytical solutions of a generalized higher-order beam equation. Proceedings of the Royal Society A **477**(2255), 20210455 (2021)

22. F.S. Khodadad, S.M. Mirhosseini-Alizamini, B. Günay, L. Akinyemi, H. Rezazadeh, M. Inc, Abundant optical solitons to the sasa-satsuma higher-order nonlinear schrödinger equation. Opt. Quant. Electron. **53**(12), 702 (2021)
23. K.K. Ali, A. Yokus, A.R. Seadawy, R. Yilmazer, The ion sound and langmuir waves dynamical system via computational modified generalized exponential rational function. Chaos Solitons Fract. **161**, 112381 (2022)
24. T. Abdulkadir Sulaiman, A. Yusuf, Dynamics of lump-periodic and breather waves solutions with variable coefficients in liquid with gas bubbles. In: Waves in Random and Complex Media, 1-14 (2021)
25. M.I. Asjad, W.A. Faridi, S.E. Alhazmi, A. Hussanan, The modulation instability analysis and generalized fractional propagating patterns of the peyrard-bishop dna dynamical equation. Opt. Quant. Electron. **55**(3), 232 (2023)
26. S.Z. Majid, M.I. Asjad, W.A. Faridi, Solitary travelling wave profiles to the nonlinear generalized calogero–bogoyavlenskii–schiff equation and dynamical assessment. Eur. Phys. J. Plus **138**(11), 1040 (2023)
27. M.M. Roshid, M.M. Rahman, H. Or-Roshid, Effect of the nonlinear dispersive coefficient on time-dependent variable coefficient soliton solutions of the Kolmogorov-Petrovsky-Piskunov model arising in biological and chemical science. Heliyon **10**(11) (2024)
28. M.M. Roshid, M.N. Alam, O.A. İlhan, M.A. Rahim, M.M.H. Tuhin, M.M. Rahman, Modulation instability and comparative observation of the effect of fractional parameters on new optical soliton solutions of the paraxial wave model. Opt. Quant. Electron. **56**(6), 1010 (2024)
29. A. Kundu, A. Mukherjee, Novel integrable higher-dimensional nonlinear Schroedinger equation: properties, solutions, applications. (2013) arXiv preprint arXiv:1305.4023
30. A. Kundu, A. Mukherjee, T. Naskar, Modelling rogue waves through exact dynamical lump soliton controlled by ocean currents. Proc. R. Soc. A: Math. Phys. Eng. Sci. **470**(2164), 20130576 (2014)
31. M. Ekici, A. Sonmezoglu, A. Biswas, M.R. Belic, Optical solitons in (2+ 1)–dimensions with kundu–mukherjee–naskar equation by extended trial function scheme. Chin. J. Phys. **57**, 72–77 (2019)
32. Y. Yıldırım, Optical solitons to kundu–mukherjee–naskar model with modified simple equation approach. Optik **184**, 247–252 (2019)
33. Y. Yıldırım, Optical solitons to kundu–mukherjee–naskar model in birefringent fibers with trial equation approach. Optik **183**, 1026–1031 (2019)
34. Y. Yildirim, Optical solitons to Kundu-Mukherjee-Naskar model with trial equation approach. Optik, 183 (2019)
35. D. Kumar, G.C. Paul, T. Biswas, A.R. Seadawy, R. Baowali, M. Kamal, H. Rezazadeh, Optical solutions to the kundu-mukherjee-naskar equation: mathematical and graphical analysis with oblique wave propagation. Phys. Scr. **96**(2), 025218 (2020)
36. A. Jhangeer, A.R. Seadawy, F. Ali, A. Ahmed, New complex waves of perturbed shrödinger equation with kerr law nonlinearity and kundu-mukherjee-naskar equation. Results Phys. **16**, 102816 (2020)
37. R.U. Rahman, M.M.M. Qousini, A. Alshehri, S.M. Eldin, K. El-Rashidy, M.S. Osman, Evaluation of the performance of fractional evolution equations based on fractional operators and sensitivity assessment. Results Phys. **49**, 106537 (2023)
38. O. González-Gaxiola, A. Biswas, M. Asma, A.K. Alzahrani, Optical dromions and domain walls with the kundu–mukherjee–naskar equation by the laplace-adomian decomposition scheme. Regular Chaotic Dyn. **25**(4), 338–348 (2020)
39. R.A. Talarposhti, P. Jalili, H. Rezazadeh, B. Jalili, D.D. Ganji, W. Adel, A. Bekir, Optical soliton solutions to the (2+ 1)-dimensional kundu–mukherjee–naskar equation. Int. J. Mod. Phys. B **34**(11), 2050102 (2020)
40. S. Singh, A. Mukherjee, K. Sakkaravarthi, K. Murugesan, Higher dimensional localized and periodic wave dynamics in a new integrable (2+ 1)-dimensional Kundu-Mukherjee-Naskar model. (2020) arXiv preprint arXiv:2001.06766
41. T.A. Sulaiman, H. Bulut, The new extended rational sgeem for construction of optical solitons to the (2+ 1)–dimensional kundu–mukherjee–naskar model. Appl. Math. Nonlinear Sci. **4**(2), 513–522 (2019)
42. H. Rezazadeh, A. Kurt, A. Tozar, O. Tasbozan, S.M. Mirhosseini-Alizamini, Wave behaviors of kundu-mukherjee-naskar model arising in optical fiber communication systems with complex structure. Opt Quantum Electron. **53**(6), 317 (2021)
43. E.M. Zayed, R.M. Shohib, M.E. Alngar, Optical solitons in bragg gratings fibers for the nonlinear (2+ 1)-dimensional kundu–mukherjee–naskar equation using two integration schemes. Opt. Quant. Electron. **54**(1), 16 (2022)
44. A. Ali, S. Javed, M. Nadeem, L.F. Iambor, S. Mureşan, A soliton solution for the kadomtsev-petviashvili model using two novel schemes. Symmetry **15**(7), 1364 (2023)
45. A. Jhangeer, T. Jamal, A.M. Talafha, M.B. Riaz, Exploring travelling wave solutions, bifurcation, chaos, and sensitivity analysis in the (3+ 1)-dimensional gkdv-zk model: a comprehensive study using lie symmetry methodology. Results Eng. **22**, 102194 (2024)
46. S.N. Ananna, T. An, M. Asaduzzaman, M.S. Rana, Sine-gordon expansion method to construct the solitary wave solutions of a family of 3d fractional wbbm equations. Results Phys. **40**, 105845 (2022)
47. M. Khater, L. Dianchen, A.M.A. Raghda, Dispersive long wave of nonlinear fractional Wu-Zhang system via a modified auxiliary equation method. AIP Adv. 9.2 (2019)
48. M.A.S. Murad, H.F. Ismael, T.A. Sulaiman, A class of optical solutions for time-fractional perturbed fokas-lenells equation via a modified sardar sub-equation approach. Opt. Quant. Electron. **56**(7), 1130 (2024)
49. N.M. Kamel, H.M. Ahmed, W.B. Rabie, Retrieval of soliton solutions for 4th-order (2+ 1)-dimensional schrödinger equation with higher-order odd and even terms by modified sardar sub-equation method. Ain Shams Eng. J. **15**(7), 102808 (2024)
50. G. Akram, M. Sadaf, M.A.U. Khan, Abundant optical solitons for lakshmanan–porsezian–daniel model by the modified auxiliary equation method. Optik **251**, 168163 (2022)
51. A.A. Mamun, C. Lu, S.N. Ananna, M.M. Uddin, Dynamical behavior of water wave phenomena for the 3d fractional wbbm equations using rational sine-gordon expansion method. Sci. Rep. **14**(1), 6455 (2024)
52. S.N. Ananna, A.A. Mamun, M.A.A. Meia, C. Lu, Chaotic behaviour, bifurcation, and stability analysis of the time-fractional phi-four model using the Hirota bilinear form. Int. J. Comput. Math., 1-21 (2025)